THESIS

SUPERHYDROPHOBIC SURFACES FOR REDUCING LIQUID ADHESION AND CONTACT TIME

Submitted by

Lewis Marinoff Boyd

Department of Mechanical Engineering

In partial fulfillment of the requirements

For the Degree of Master of Science

Colorado State University

Fort Collins, Colorado

Summer 2017

Master's Committee:

Advisor: Arun K. Kota

Ketul Popat
Melissa Reynolds

ABSTRACT

SUPERHYDROPHOBIC SURFACES FOR REDUCING LIQUID ADHESION AND CONTACT TIME

Superhydrophobic surfaces are extremely repellent to water and aqueous liquids. Water droplets can bead up, bounce and easily roll off from superhydrophobic surfaces. Consequently, superhydrophobic surfaces can be used to reduce liquid adhesion to food containers and manufacturing equipment which is a significant problem for food packaging and agricultural industries.

In this work, in order to reduce liquid waste in food containers, a novel superhydrophobic coating made with natural, edible materials was developed and fabricated. The superhydrophobic coatings made with edible materials virtually eliminate liquid waste in food containers. Systematic experiments were conducted on superhydrophobic coatings and non-textured, low adhesion films to evaluate the performance of the coatings and films in reducing liquid adhesion to manufacturing equipment. In high shear environments such as manufacturing equipment, non-textured, low adhesion films perform better than superhydrophobic coatings due to their improved durability.

Further, superhydrophobic surfaces can be used to reduce the time an impacting liquid droplet is in contact with the surface (contact time), which in turn is useful for anti-icing applications. In this work, superhydrophobic surfaces with and without macroscale texture were design, fabricated and evaluated for their contact time with water droplets. The contact time was significantly lower on macroscale textured superhydrophobic surfaces (i.e., better for anti-icing) compared with superhydrophobic surfaces without macroscale texture.

ACKNOWLEDGEMENTS

While the individuals that have assisted me in creating this work are too numerous to count, I would like to acknowledge the following individuals who have directly helped with this work.

Thank you to all fellow graduate students and the whole research group, particularly Darryl Beemer, Sanli Movafaghi, Hamed Vahabi, Anudeep Pendurthi, Sravanthi Vallabhuneni, Matt Cackovic and Wei Wang for providing engaging discussions and illuminating instructions. Thank you to the Khetani group and specifically to Matthew Davidson for collaborating in this work. Thank you to Dr. Arun Kota for all of the hours and effort in advising this work while providing a guiding light past troublesome obstacles.

TABLE OF CONTENTS

1 INTRODUCTION

Superhydrophobic surfaces are extremely repellent to water and aqueous liquids and have received significant interest in recent years due to their applications in a wide variety of industries including energy production/transmission, transportation, agriculture, consumer products and medical devices. This interest is propelled by careful examination of natural repellent surfaces using cutting edge imaging and analysis methods which lead to a fundamental understanding of repellent surfaces and the capability to fabricate engineered repellent surfaces. Superhydrophobic surfaces shed water very easily and it is difficult to balance a water droplet on the surface. The design criteria of superhydrophobic, superoleophobic (extremely repellent to oil) and superomniphobic (extremely repellent to virtually all liquids) surfaces are presented in chapter 2.

Superhydrophobic surfaces have a variety of potential applications due to their capability to reduce liquid adhesion, for example food packaging and manufacturing equipment. The design, fabrication and performance of a novel coating for reducing liquid adhesion to food containers is presented in chapter 3.

Liquid adhesion of agricultural seed dressing to manufacturing equipment is a concern because the adhered liquid reduces processing efficiency and increases cleaning costs. A systematic study of liquid adhesion on superhydrophobic and superomniphobic (ultra-low adhesion) coatings and non-textured low adhesion films is presented in chapter 4.

Superhydrophobic coatings have also received interest due to their anti-icing potential by reducing the time an impinging liquid droplet is in contact with the surface. Ice accumulation on airplanes is a significant hazard to human safety and the buildup of ice on car windshields is an annoyance in winter climates. Superhydrophobic surfaces with and without macroscale texture

were fabricated and evaluated for the time of contact of impinging water droplets at a variety of impact velocities in chapter 5.

Potential areas of new investigations for each topic of study are detailed in future work presented in chapter 6.

2 BACKGROUND

2.1 Wettability

The wettability of a surface is typically characterized by a liquid's contact angle and contact angle hysteresis on the surface. The wettability of non-textured (e.g., smooth) surfaces is fundamental to the understanding of all repellent surfaces and the focus of the earliest wetting analyses. For a smooth surface, Young's relation[6] defines the equilibrium contact angle θ for a liquid:

$$\cos\theta = \frac{\gamma_{SV} - \gamma_{SL}}{\gamma_{LV}} \tag{2.1}$$

Here, γ_{SV} is the solid surface energy, γ_{LV} is the liquid surface tension and γ_{SL} is the solid-liquid interfacial energy. Young's equation arises from the force balance for a liquid droplet contacting a non-textured, non-reactive (e.g., no strong chemical bonds formed due to interactions between liquid and solid) solid surface and can be visualized in **Figure 2.1**. The contact angle is defined as the angle between the tangent to the liquid-vapor interface and the tangent to the liquid-solid interface at the triple phase contact line, measured through the liquid. For a given liquid, a lower solid surface energy will result in higher contact angles than a higher solid surface energy.[3,7,8] Therefore, lower surface energy materials are preferred for repellent-surfaces. The lowest surface energy materials are typically fluorinated or perfluorinated materials. A surface with $\theta > 90°$ is

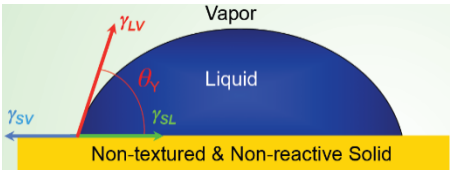

Figure 2.1. *Schematic of energy balance at the triple-phase contact point for a liquid drop on a non-textured surface.*[1]

considered to be hydrophobic and a surface with $\theta < 90°$ is considered to be hydrophilic. The highest observed water contact angle on even the lowest γ_{SV} non-textured surface is $\theta \approx 130°$.[9] Higher contact angles can be achieved with textured surfaces.[10,11]

2.2 Designing Superhydrophobic Surfaces

When a liquid droplet contacts a textured surface, it displays a macroscopic apparent contact angle θ^* which is used for analysis of textured surfaces. The textured surfaces exhibit local contact angles that follow Young's contact angle for a flat surface but these contact angles are constrained to the micro and nano-texture and do not fully represent the textured surface. A liquid droplet on a textured surface adopts one of the two possible states – Wenzel[12] state or Cassie-Baxter[13] state. In the Wenzel state, the liquid penetrates the texture and wets the surface completely (**Figure 2.2**). The apparent contact angle in the Wenzel state (θ_W^*) can be predicted by:

$$\cos\left(\theta_W^*\right) = r\cos\theta \tag{2.2}$$

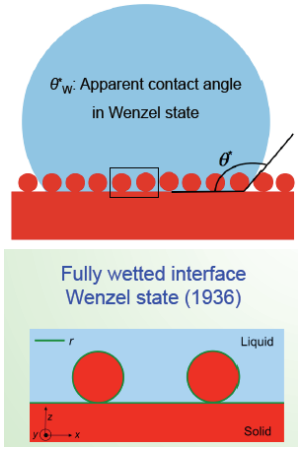

Figure 2.2. *Schematic of a liquid drop in the Wenzel state on a textured surface.*[1]

Where θ is the contact angle on a flat surface of the same material and r is the roughness factor defined as the ratio of the actual surface area to the geometric (or projected flat) surface area. For real surfaces, r is always greater than unity; however, polished and other reasonably flat surfaces,

(e.g., flat glass, silicon wafers, Teflon™ and mirror-polished metals) are reasonably modeled with roughness factors of $r = 1$. Based on equation 2.2, a surface with $\theta > 90°$ displays $\theta^*_W > \theta > 90°$. Conversely, a liquid with $\theta < 90°$ displays $\theta^*_W < \theta < 90°$. Therefore, the Wenzel state increases the hydrophobicity of a hydrophobic surface and increases the hydrophilicity of a hydrophilic surface.

In the Cassie-Baxter state, air pockets are trapped between the surface and the liquid; therefore, the liquid contacts both air and solid (**Figure 2.3**). The apparent contact angle θ^*_{CB} for a droplet in the Cassie state is given by:

$$\cos(\theta^*_{CB}) = f_{SL}\cos\theta + f_{LV}\cos\pi \qquad (2.3)$$

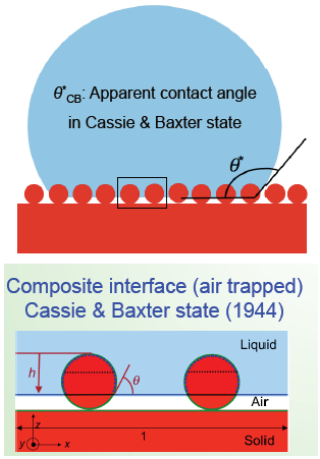

Figure 2.3. *Schematic of a liquid drop in the Cassie-Baxter state on a textured surface.*[1]

Where f_{SL} is the solid fraction of the interface and f_{LV} is the vapor fraction of the composite drop interface. As f_{LV} increases, θ^*_{CB} increases. The Cassie-Baxter state is preferred for designing superhydrophobic surfaces[10,14] because the air pockets reduce the *S-L* contact area and result in high apparent advancing (maximum) contact angles θ^*_{adv}, high apparent receding (minimum) contact angles θ^*_{rec}, and low contact angle hysteresis $\Delta\theta$ (difference between advancing and receding contact angle on a given solid surface).

2.2.1 Contact Angle Hysteresis

The contact angle hysteresis ($\Delta\theta$) for a surface is the second parameter for analyzing surfaces. A very low $\Delta\theta$ indicates a very homogeneous surface (both chemically and physically). Conversely, a very high $\Delta\theta$ indicates a very inhomogeneous surface. A surface is considered to be superhydrophobic when θ^* >150° and $\Delta\theta \leq 10°$ with water.[3,7,8,15,16] The low $\Delta\theta^*$ leads to a low roll off angle ω (minimum angle of tilt relative to horizontal for droplet to roll off of a surface).[17]

2.3 Designing Superomniphobic Surfaces

Superhydrophobic surfaces can repel water and aqueous liquids, however they typically cannot repel low surface tension liquids (e.g., oils) because lower surface tension liquids have lower contact angles on a given solid surface compared to higher surface tension liquids. The Cassie-Baxter state is also preferred for designing superoleophobic (extremely repellent to oil) surfaces[10,14,18-20] because the air pockets reduce the solid-liquid contact area and result in high apparent advancing contact angles θ^*_{adv}, high apparent receding contact angles θ^*_{rec} and low contact angle hysteresis. However, superoleophobicity requires a specific type of texture called re-entrant (i.e., multivalued surface topography, see **Figure 2.4a** and **b**).[21-23] The re-entrant texture allows a droplet to adopt a nanoscale contact angle < 90° on the surface which is necessary for superoleophobicity because low surface tension liquids have Young's contact angle θ < 90° on virtually all surfaces.

A surface is considered to be superhydrophobic when apparent contact angle > 150° and contact angle hysteresis is low for water[3,7,8,15,16] and superoleophobic when apparent contact angle >150° and contact angle hysteresis is low for low surface tension liquids (e.g., oils). When a surface is both superhydrophobic and superoleophobic, is it called superomniphobic (extremely repellent to virtually all liquids).[24-26]

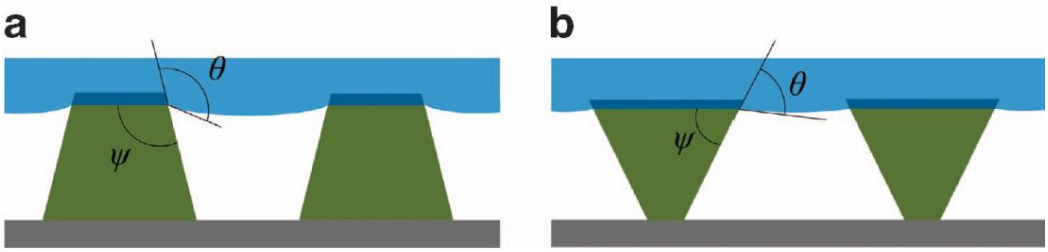

Figure 2.4. *a) Surface texture without multivalued surface topography, only suitable for superhydrophobicity. b) Surface texture with multivalued surface topography, can be superoleophobic and superhydrophobic.*[3]

3 EDIBLE SUPERHDYROPHOBIC COATINGS

3.1 Literature Review and Background

3.1.1 Introduction

In daily life, there can be a significant (up to 15%) waste of liquid food products as residue in food containers.[27] This waste occurs because liquids (e.g., soup, liquid margarine and honey) remain adhered to the container after use. One strategy to reduce the liquid waste is to employ superhydrophobic coatings (i.e., coatings that are extremely repellent to water), which have tremendous practical applications, including self-cleaning and drag reduction.[3,7,8,28-32] Superhydrophobic coatings are fabricated through a combination of surface texture (e.g., micro-scale texture or nano-scale texture or hierarchical texture) and chemical modification that imparts low solid surface energy. They can reduce liquid waste by lowering the adhesion between the container and aqueous liquids. Typically, superhydrophobic coatings are fabricated using fluorocarbon materials, which possess low surface energy.[25,31,32] The U.S. Environmental Protection Agency (EPA) classifies long chain fluorocarbon materials as "emerging contaminants" because of their potential decomposition into perfluorooctanoic acid (PFOA),[33] which is considered persistent, bioaccumulative and potentially toxic to humans.[34,35] Therefore, superhydrophobic coatings fabricated using fluorocarbon materials are not ideal for direct food contact applications. Further, the use of coatings in food related applications is regulated by the U.S. Food and Drug Administration (FDA). To make a superhydrophobic coating for a food container, the materials in the coating should be non-toxic and classified as safe for direct food contact by the FDA. There are very few reports of superhydrophobic surfaces fabricated with materials for direct food contact.[36] The ideal material for food related applications of a

superhydrophobic coating should preferably be edible because of potential leaching of the coating material. To the best of our knowledge, there are no reports of superhydrophobic coatings fabricated with natural, edible materials using a simple, low cost, scalable, single step process. In this work, we used natural, edible materials to fabricate superhydrophobic coatings that water and aqueous liquids (e.g., Lipton® green tea, Gatorade™, pancake syrup, Coca-Cola™, orange juice, milk and coffee) can bounce and roll off from. We demonstrate that such superhydrophobic coatings are effective for significantly reducing and even eliminating food residue inside a container. Further, our toxicity tests indicate that there are no significant effects on the viability of cells *in vitro* from leaching of the coating material. We envision that our methodology will have applications in reducing the waste from viscous food liquids, pharmaceutical liquids and medical liquids adhering to the container after use.

3.1.2 Background

As discussed in chapter 2, low solid surface energy and texture are necessary for a droplet to adopt the Cassie-Baxter state on a surface which is preferred for designing superhydrophobic surfaces. In this work, we fabricated superhydrophobic coatings with two types of natural, edible materials–carnauba wax (γ_{SV} = 24 mN m^{-1}) and beeswax (γ_{SV} = 28 mN m^{-1}) (see section 3.2.1). We selected these materials because they are classified by the FDA as GRAS (generally recognized as safe; 21CRF184.1978, 21CFR184.1973),[37] and have a low γ_{SV} (see section 3.2.6). We imparted micro-scale texture to these materials via a simple, low cost, scalable spray coating process (see section 3.2.1). The low solid surface energies of carnauba wax and beeswax combined with the micro-scale surface texture results in superhydrophobicity.[38,39]

3.2 Materials/Methods/Experiments

3.2.1 Spray Coating

We fabricated our superhydrophobic coatings with carnauba wax (Strahl & Pitsch, Inc.) and beeswax (S. C. Johnson, Inc.) via spray coating 20 mg mL^{-1} wax-in-acetone emulsions (prepared via ultrasonication). Glass slides (7.5 cm x 2.5 cm) were cleaned with piranha solution, thoroughly rinsed with deionized water and subsequently dried using nitrogen gas. The wax-in-acetone emulsions were sprayed onto the non-textured substrates (glass slides) which were held at a distance of ~12 cm from the spray coater nozzle. The pressure during spray coating was held constant at ~30 psi.

3.2.2 Contact and Roll Off Angle, Surface Tension and Energy Measurements

Advancing contact angle, receding contact angle, roll off angle and surface tension measurements were conducted using a Ramé-Hart 260-F4 goniometer and tensiometer. Advancing contact angles and receding contact angles were measured by advancing or receding a small volume of liquid (~8 µL) on the surface using a 2 mL micrometer syringe (Gilmont). Roll off angles were measured by tilting the stage until the droplet (~8 µL) rolled off from the surface. For each liquid, at least five measurements were performed on each surface. The contact angle and roll off angle measurement uncertainty was ±1º and ±0.5º, respectively. The pendant drop method was used to measure surface tension of different liquids. At least five surface tension measurements were performed for each liquid and the measurement uncertainty was ±1 mN m^{-1}. Owens-Wendt analysis was used to estimate the solid surface energy of the coating materials.

3.2.3 Bouncing Droplet Imaging

High-speed movies were obtained using a Photron Fastcam SA3 camera at 2000 frames per second.

3.2.4 Scanning Electron Microscopy

Images were taken with a JEOL-6500F SEM (scanning electron microscope) at 5 kV at a working distance of 11.5 mm.

3.2.5 Toxicity Tests

3T3-J2 fibroblasts[40] were seeded at a density of 300,000 cells mL^{-1} into 96 well tissue culture plates. Cells were maintained for 7 days prior to wax medium incubations, with the medium changed every 3 days to supply the cells with fresh nutrients. The cell culture medium was composed of Dubelco's Modified Eagle medium (DMEM, Corning) that contained phenol red, 4.5 g L^{-1} glucose, 3 mM L-glutamine (Corning), 10% vol/vol bovine serum (Thermo-Fisher), and 1% vol/vol penicillin/streptomycin (Corning). Wax was incubated in cell culture medium at 37 ºC for 7 days. After 7 days incubation, samples were centrifuged at 1000 *g*, supernatants were removed and sterile filtered through a 0.2 µm cellulose acetate syringe filter. This medium was diluted into a cell culture medium incubated under the same conditions except without wax. The cell culture medium was removed from the cells and various concentrations of wax-incubated medium were added to the cells. A live/dead stain was performed on the cells after 24 hours of incubation with a cell *permeant* blue dye (Hoechst 33342) that stains the DNA inside all of the cells (live or dead), and a cell *impermeant* red dye (propidium iodide) that stains the DNA of only those cells that have compromised outer membranes (i.e., dead). In particular, kit reagents (ReadyProbes Cell Viability Imaging Kit, Thermo-Fisher) were diluted into cell culture medium according to manufacturer's specifications and incubated with cell samples for 15 minutes at 37 ºC. Images were acquired using phase contrast as well as the RFP (red fluorescent protein) and DAPI (4',6-diamidino-2-phenylindole, dihydrochloride) LED light cubes on an EVOS FL microscope (Thermo-Fisher). After imaging, ATP levels inside the cells were quantified using a Promega Cell Titer Glo 2.0 kit.

Briefly, 'Cell Titer Glo reagent' was added to cells and the luminescent signal was quantified using a Synergy H1 multi-mode luminometer (Biotek).

3.2.6 Solid Surface Energy

Owens-Wendt[41] approach was used to estimate the solid surface energy γ_{SV} of the edible coating materials. Rapeseed oil (γ_{LV} = 35 mN m^{-1}) was used as the non-polar liquid to estimate the dispersive component of the solid surface energy γ_{SV}^{d} and water (γ_{LV}^{d} = 21.1 mN m^{-1} and γ_{LV}^{p} = 51.0 mN m^{-1}) was used as the polar liquid to estimate the polar component of the solid surface energy γ_{SV}^{p}. The advancing contact angles θ_{adv} measured on non-textured edible material-based surface were used to estimate the solid surface energy (**Table 3.1**).[42] It is worth noting that the low solid surface energies of carnauba wax and beeswax confirm the hydrophobic nature of these materials, as reported in prior studies.[43-45]

Table 3.1. Surface energy γ_{SV} of the edible coating materials used in this work.

Material	θ_{water}^{adv} (°)	$\theta_{rapeseed\_oil}^{adv}$ (°)	γ_{SV} (mN m^{-1})
Carnauba Wax	113	50	24
Beeswax	110	40	28

3.2.7 Liquid Surface Tension

Liquids with various surface tensions were mimicked by adding various amounts of SDS (sodium dodecyl sulphate) to water. Pendant drop method was used to measure the surface tension of liquid (**Table 3.2**).

Table 3.2. Surface tension γ_{LV} of various concentrations of water and SDS (sodium dodecyl sulphate).

SDS Concentration (mM)	γ_{LV} (mN m^{-1})
0	72
1.04	67
2.25	59
3.12	53
4.98	46
6.07	42
10.06	37

It is worth noting here that SDS in water solutions are good mimics of edible liquids for evaluating the contact angles and roll off angles although the viscosity of SDS in water solutions may be significantly lower than that of edible liquids. This is because viscosity has negligible influence (if any) on the contact angles and roll off angles of liquids, as evident from equation 2.1 and Furmidge's relation (see section 3.3.2).

3.2.8 Maximum Concentration of Leached Coating

Consider a cylindrical container of radius r = 2.5 cm and height h = 15 cm. The internal surface area, including side walls and bottom surface, is given as:

$$A_{\text{int}ernal} = 2\pi rh + \pi r^2 \approx 225\,\text{cm}^2 \tag{3.1}$$

The amount of carnauba wax required to impart a superhydrophobic coating is given as (assuming ρ_s = 0.7 mg cm^{-2}):

$$m_{coating} = \rho_s A_{internal} \approx 179\,\text{mg} \tag{3.2}$$

Assuming that all of the coating material leaches into the liquid product and is ingested, the concentration of carnauba wax in the bloodstream can be computed as (assuming human body has V = 5 L of blood):

$$C = \frac{m_{coating}}{V} \approx 0.04\,\text{mg mL}^{-1} \tag{3.3}$$

The highest concentration (500 mg mL^{-1}) of carnauba wax used in the toxicity test was four orders of magnitude higher than this.

3.3 Results and Discussion

3.3.1 Superhydrophobicity

In order to identify the conditions necessary to completely coat a surface and impart superhydrophobicity, we investigated θ^*_{adv} and θ^*_{rec} for water as a function of coating surface density ρ_s (mass of the coating per unit area). When a non-textured surface (e.g., glass slide; see **Figure 3.1a**) is coated with carnauba wax at ρ_s < 0.55 mg cm^{-2}, it leads to low θ^*_{adv} and θ^*_{rec} and high $\Delta\theta^*$ (**Figure 3.1d**) for water because of insufficient surface coverage (**Figure 3.1b**). At $\rho_s \approx$ 0.55 mg cm^{-2}, it leads to high θ^*_{adv} and θ^*_{rec} and low $\Delta\theta^*$ (**Figure 3.1d**) for water because of complete surface coverage (**Figure 3.1c**) with the desired roughness. Increasing ρ_s further increases the coating thickness, but does not alter the roughness significantly. Consequently θ^*_{adv} and θ^*_{rec} do not change significantly for $\rho_s \gtrsim$ 0.55 mg cm^{-2}. In this manner, with sufficiently high ρ_s,

we fabricated superhydrophobic coatings with carnauba wax (θ^*_{adv} = 162°, θ^*_{rec} = 159° for water; **Figure 3.1e**) as well as beeswax (θ^*_{adv} = 155°, θ^*_{rec} = 145° for water; **Figure 3.1f**).

One application of our edible superhydrophobic coatings is to reduce the liquid waste in food containers. Many liquid products consumed daily have lower γ_{LV} than water (γ_{LV} = 72 mN m^{-1}), such as (Lipton® green tea [γ_{LV} = 69 mN m^{-1}], Gatorade™ [γ_{LV} = 68 mN m^{-1}], pancake syrup [γ_{LV} = 68 mN m^{-1}], Coca-Cola™ [γ_{LV} = 57 mN m^{-1}], orange juice [γ_{LV} = 57 mN m^{-1}], milk [γ_{LV} =

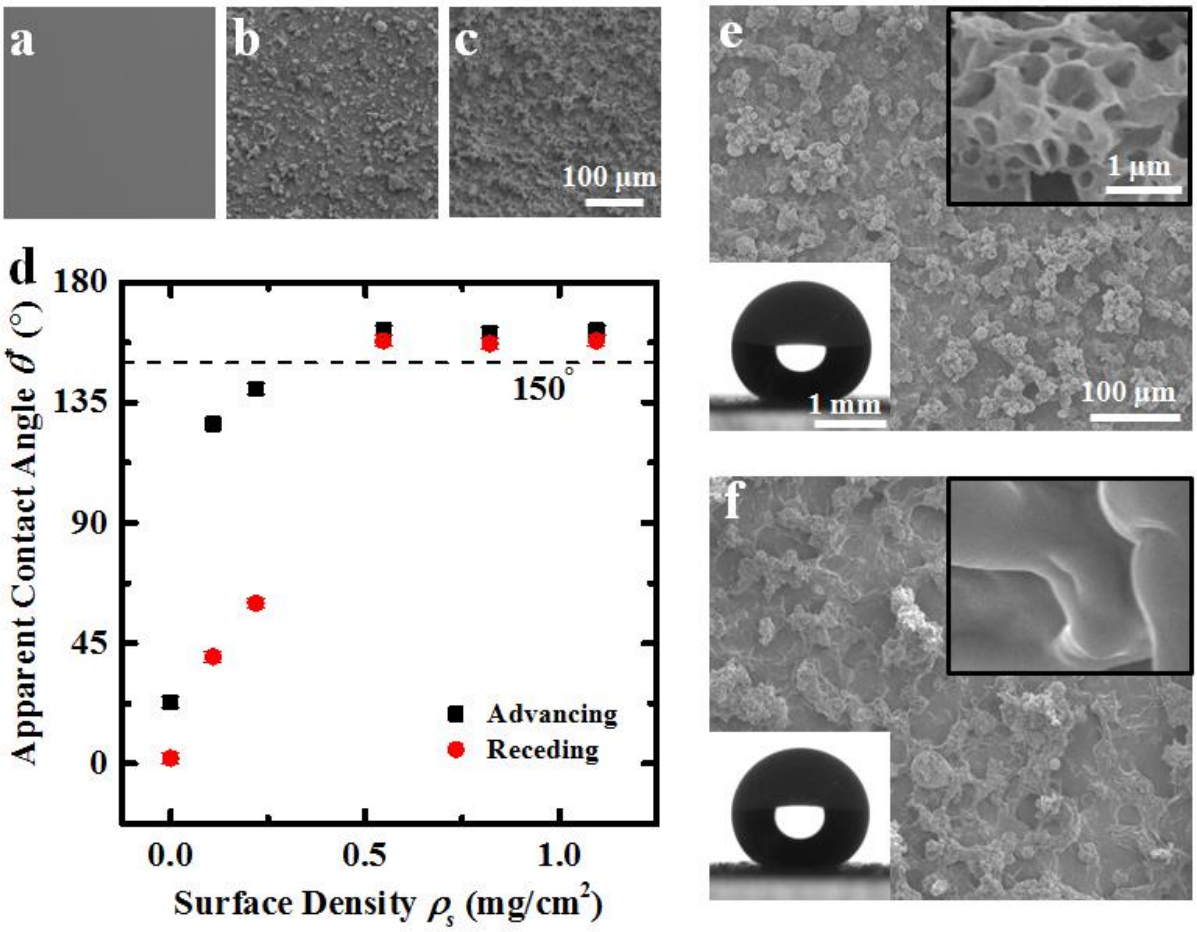

Figure 3.1. *a), b) and c) Glass slide coated with 0, 0.2 and 0.55 mg cm^{-2} of emulsion, respectively. d). Advancing and receding apparent contact angles of water on a glass slide coated with varying ρ_s of carnauba wax. The surface becomes superhydrophobic when $\rho_s \gtrsim$ 0.55 mg cm^{-2}. e and f) Scanning electron microscope (SEM) images of glass slides coated with 0.55 mg cm^{-2} of carnauba wax and 1.1 mg cm^{-2} of beeswax, respectively. The upper right inset of each frame shows a higher magnification image of the micro-scale structures and the lower left inset shows θ^* > 150° for both coating materials.*

48 mN m^{-1}] and coffee [γ_{LV} = 46 mN m^{-1}]). In order to validate that our edible superhydrophobic coatings can effectively reduce liquid waste in food containers, we evaluated the wetting behavior (θ^*_{adv}, θ^*_{rec}, and ω) of liquids with different γ_{LV} on our edible superhydrophobic coatings. We employed water with various concentrations of sodium dodecyl sulfate (SDS) to mimic edible liquids with different γ_{LV} (section 3.3.2). Our results indicate that liquids with γ_{LV} > 45 mN m^{-1} display θ^*_{adv} > 150° (**Figure 3.2a**) and ω < 10° (**Figure 3.2b**) on superhydrophobic coatings fabricated using carnauba wax. We obtained similar results with superhydrophobic coatings fabricated using beeswax. This suggests that our superhydrophobic coatings fabricated using edible materials can effectively repel common liquid products consumed daily. The measured ω

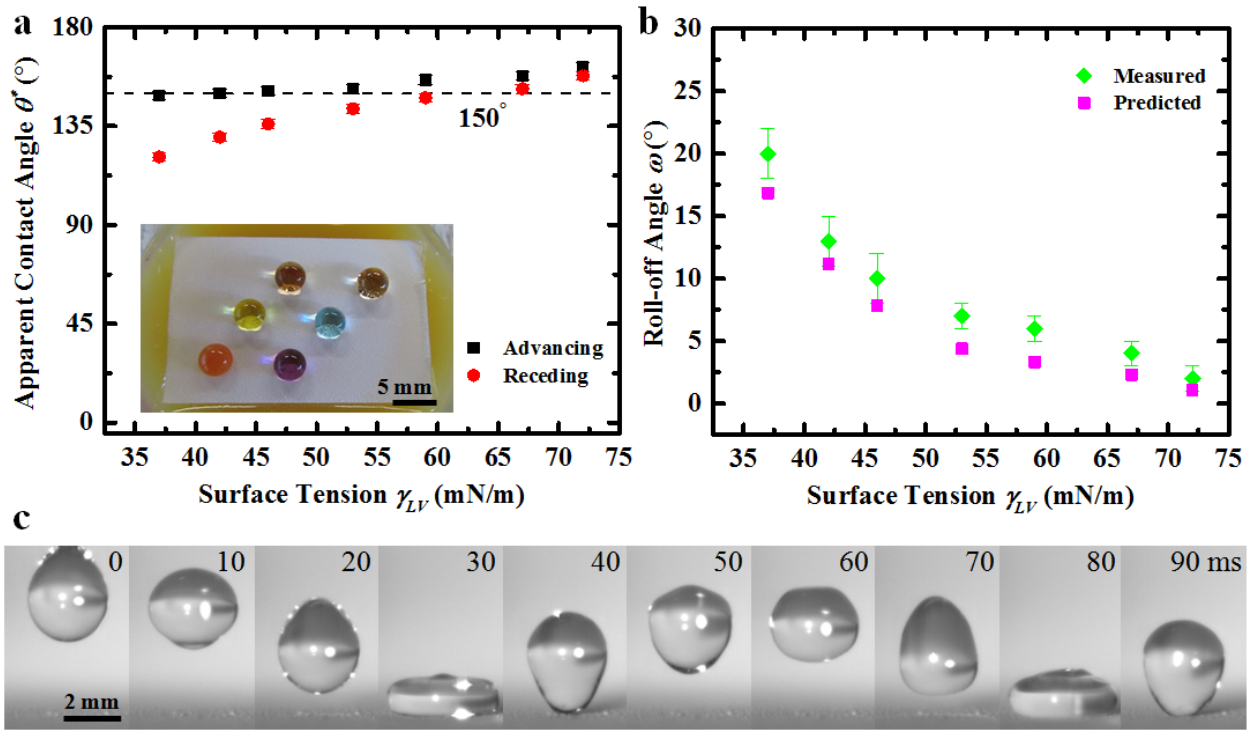

Figure 3.2. *a) Advancing and receding apparent contact angles for various* γ_{LV}*, water + SDS solutions on carnauba wax coatings. Inset shows common liquid products beading up on the surface of a carnauba wax coated glass slide floating in orange juice (liquids from left to right, bottom row: ketchup and water, middle row: Lipton® green tea and Gatorade™, top row: Coca-Cola™ and pancake syrup. b)* ω *of various* γ_{LV} *water + SDS solutions on carnauba wax coating. c) Series of snapshots showing a 14 μL water droplet bouncing on a carnauba wax coating.*

values match well with our predictions based on a balance between work done by gravity and the work expended due to adhesion (**Figure 3.2b** and see section 3.3.2). Further, the high θ^*_{adv} and low ω allow liquid droplets to easily bounce on our superhydrophobic coatings (**Figure 3.2c**).

3.3.2 Roll Off Angles

Based on a balance between work done by gravitational force and work expended due to adhesion, the roll off angle ω (**Figure 3.3**) on a super-repellent surface is given as:[6]

$$\rho g V \sin\omega \approx \gamma_{LV} D_{TCL}\left(\cos\theta^*_{rec} - \cos\theta^*_{adv}\right) \tag{3.4}$$

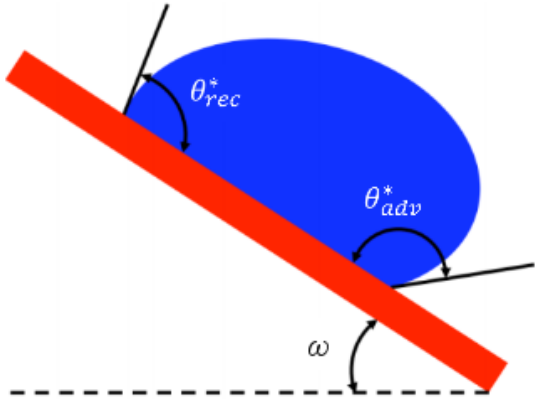

Figure 3.3. *A schematic illustrating a drop on a textured surface tilted at an angle* ω *relative to the horizontal.*

Here, γ_{LV}, ρ and V are surface tension, density and volume of the liquid droplet, respectively, and g is the acceleration due to gravity, θ^*_{adv} and θ^*_{rec} are the apparent advancing contact angle and the apparent receding contact angle, respectively, and D_{TCL} is the width of the triple phase contact line perpendicular to the rolling direction. When the shape of the droplet does not deviate significantly from a spherical cap, the width of the triple phase contact line can be computed as:[7]

$$D_{TCL} = 2\cos\left(\bar{\theta}^* - \frac{\pi}{2}\right)\left[\frac{3V}{\pi\left(2 - 3\cos\bar{\theta}^* + \cos^3\bar{\theta}^*\right)}\right]^{1/3} \tag{3.5}$$

Here, $\bar{\theta}^*$ is the average apparent contact angle, given as:

$$\cos\bar{\theta}^* = \frac{\cos\theta^*_{adv} + \cos\theta^*_{rec}}{2} \quad (3.6)$$

The estimated roll off angles of ~8 μL droplets of different liquids shown in **Figure 3.2b** were obtained using equations 3.4, 3.5 and 3.6 and listed in **Table 3.3**.

Table 3.3. Predicted and measured ω values for superhydrophobic coatings with carnauba wax.

γ_{LV} [mN m^{-1}]	ω (measured) [°]	ω (predicted) [°]
72	2	1.1
67	4	2.3
59	6	3.3
53	7	4.4
46	9	7.8
42	13	11.2
37	20	16.8

3.3.3 Coating Performance

In order to demonstrate practical utility, we coated common polystyrene cups with our superhydrophobic coatings fabricated using carnauba wax and beeswax. Subsequently, we filled the cups with a wide variety of common liquid products consumed daily, including high viscosity liquids such as honey and chocolate syrup (**Figure 3.4a**). Upon pouring out the liquids, the coated cups facilitated easy removal of liquids with virtually no residue. In contrast, uncoated cups have significant liquid residue remaining in them (**Figure 3.4b**). These results indicate that our superhydrophobic coatings are effective in reducing liquid waste from products consumed daily.

3.3.4 Toxicity

In order to evaluate the potential health impacts due to leaching of our coating materials, we conducted toxicity experiments by exposing 3T3-J2 murine embryonic fibroblasts to coating concentrations well above the maximum expected coatings concentration due to leaching. We selected 3T3 cells since they are commonly used for assessing any potential toxicities of a wide variety of materials due to their ease of propagation *in vitro* and an ability to culture the cells in a high-throughput screening format.[46] Here, we first determined the maximum coating concentration due to leaching to be 0.04 mg mL^{-1} (see section 3.2.5). However, to account for the variability observed in inter-individual exposures,[47] we selected concentrations of coating materials up to 4 orders of magnitudes higher than the expected leaching concentration. Next, we conditioned cell culture medium with carnauba wax for 7 days (i.e., by immersion of wax in the aqueous medium), and then exposed fibroblasts to this wax-conditioned medium for 24 hours. As a measure of cell viability, we quantified the relative intracellular adenosine triphosphate (ATP) levels in fibroblast lysates and compared them to levels measured in a control condition in which fibroblasts were exposed to a non-wax-conditioned culture medium. ATP was selected because it is a critical source of energy inside cells and without such a source, cells, tissues and organisms can undergo apoptosis and/or necrosis (i.e., death). Furthermore, *in vitro* measurement of ATP has been shown to be highly useful and sensitive for the assessment of material/compound toxicities.[47] Our results indicate that intracellular ATP is not significantly altered with carnauba wax concentrations ranging from 0.01 mg mL^{-1} to 500 mg mL^{-1} when compared to a control (with no carnauba wax, i.e., 0 mg mL^{-1}) (**Figure 3.4c**).

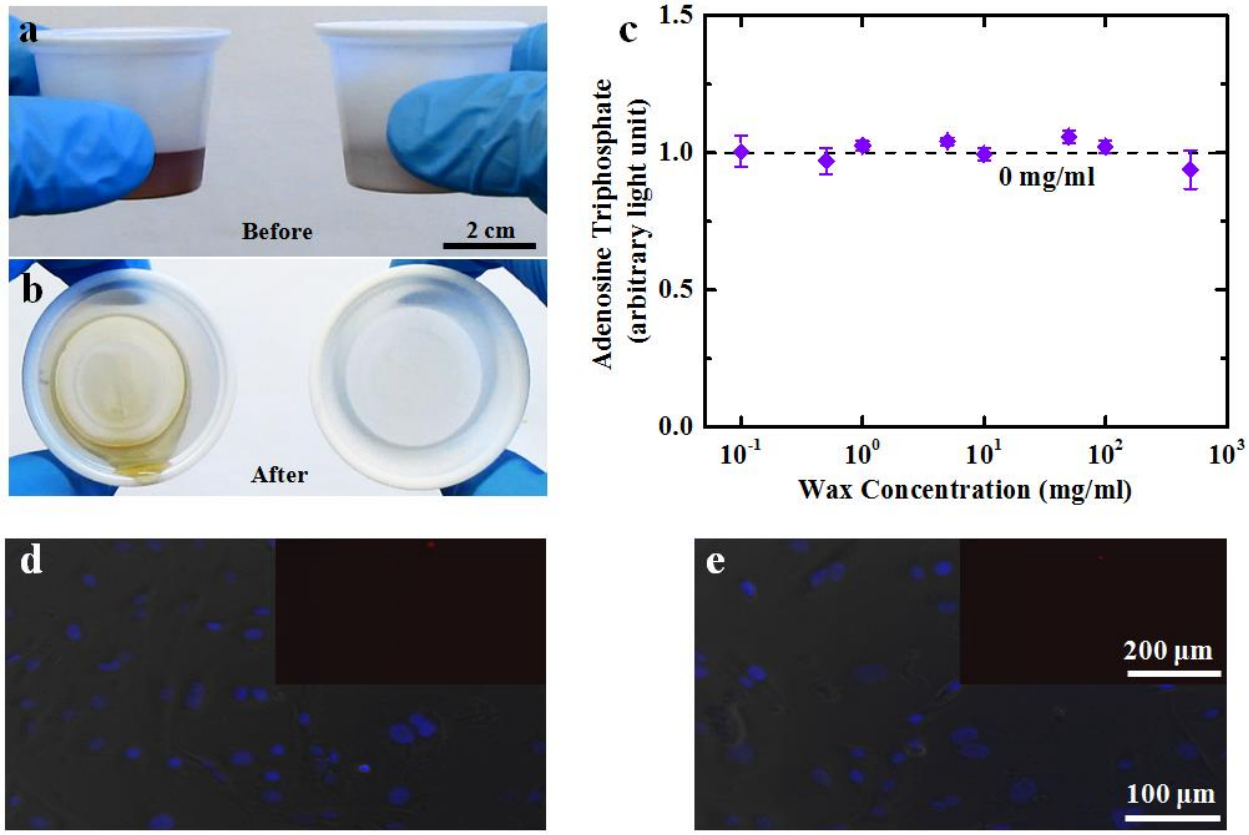

Figure 3.4. *a) Representative image of liquid in an uncoated cup (left) and carnauba wax coated cup (right). b) Residue after pouring the liquid out. c) ATP production measured from fibroblast cells exposed to various concentrations of carnauba wax and a control (0 mg mL^{-1}, dashed line). d) and e) Image of a live/dead stain of d) control cells and e) 500 mg mL^{-1} carnauba wax (all cells are blue, dead cells are red).*

In order to corroborate the aforementioned ATP findings, we simultaneously stained the cultures with two fluorescent dyes: a cell *permeant* blue dye (Hoechst 33342) that stains the nuclear DNA of all of the cells (live or dead), and a cell *impermeant* red dye (propidium iodide) that stains the nuclear DNA of only those cells that have compromised outer membranes (i.e., dead). As with ATP levels, we found that there is no significant difference in the viability of fibroblasts treated with carnauba wax concentrations up to 500 mg mL^{-1} as compared to the control (**Figure 3.4d** and **e**). We obtained similar results with beeswax as well. It is evident from the results

above that our superhydrophobic coatings fabricated with edible materials are non-toxic to a key cell type such as fibroblasts.

3.4 Conclusions

In conclusion, we used natural, edible materials to fabricate superhydrophobic coatings with a scalable, low cost, single-step technique. We fabricated coatings ($\rho_s \gtrsim 0.55$ mg cm^{-2}) with edible materials that exhibit high θ^*_{adv} and θ^*_{rec} and low $\Delta\theta^*$ for water. Further, we demonstrate that liquids with $\gamma_{LV} > 45$ mN m^{-1} display $\theta^*_{adv} > 150°$ and $\omega < 10°$ on our superhydrophobic coatings. Our toxicity tests based on ATP and fluorescent staining of live and dead cells indicate that our superhydrophobic coatings fabricated with edible materials are non-toxic to cells at coating concentrations up to four orders of magnitude higher than the maximum expected coating concentration due to leaching. While our edible superhydrophobic coatings display reasonable mechanical durability against liquids flowing past the surface, they do not have sufficient mechanical durability to withstand harsh and abrasive environments. Efforts are currently underway to improve the mechanical durability as well as the adhesion of our edible superhydrophobic coatings to various substrates. We envision that our methodology will have applications in reducing the waste from viscous food liquids, pharmaceutical liquids and medical liquids adhering to the container after use.

4 REDUCING LIQUID ADHESION FOR AGRICULTURAL EQUIPMENT

4.1 Literature Review and Background

4.1.1 Introduction

Adhesion of liquids to solid surfaces is a problem in a variety of industries (e.g., agriculture, food and fuel transportation).[48,49] Liquids typically adhere to transporting containers (e.g., pipes and tanks) and manufacturing equipment, which increases cleaning costs and reduces process efficiency. Further, liquid adhesion is often a detriment to product quality. For example, some agriculture seeds are treated before planting. This treatment is performed for a variety of reasons including improved seed germination.[50] In a typical seed treatment process, seeds are coated with an organic polymer (seed dressing), travel through a stainless-steel hopper and a heated drying rack before they are bagged for delivery. The seed dressing often adheres to the stainless-steel hopper and the drying rack (**Figure 4.1a**) and leads to seed agglomeration on the surface (**Figure 4.1b**). This leads to reduced efficiency and quality of the final seed product in addition to increased cleaning costs and labor to remove the buildup of seed dressing.

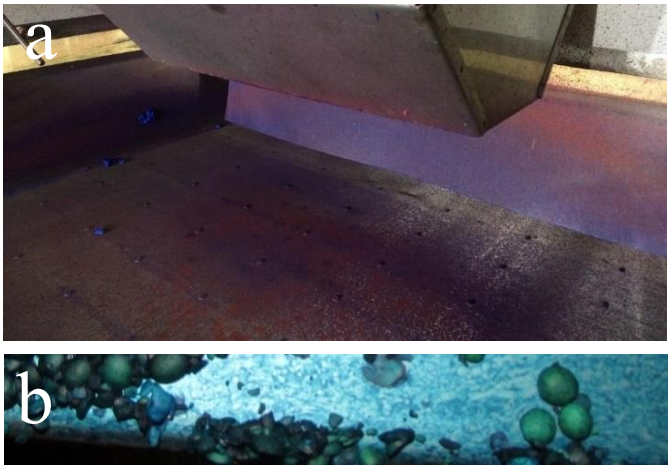

Figure 4.1. *a) Seed treatment dryer with seed dressing buildup. b) Seed agglomeration in seed treatment hopper after 3 hours of operation.*

Current seed treatment equipment uses neat stainless steel which has high adhesion to the seed dressing. In this work, we employ ultra-low adhesion coatings and low adhesion films on stainless steel to reduce seed dressing buildup. The ideal solution is to employ a durable, ultra-low adhesion coating. There are many ultra-low adhesion coatings being developed (e.g., superhydrophobic[51,52] and superomniphobic coatings[7,53,54]) and low adhesion films (non-textured, low solid surface energy films). Superhydrophobic coatings (extremely repellent to water) have ultra-low adhesion to water, superomniphobic coatings (extremely repellent to virtually all liquids) have ultra-low adhesion to virtually all liquids and non-textured, low solid surface energy films (e.g., Teflon^{TM}) have low adhesion to contacting liquids.[3,7,8,28-32]

In this work, we investigated the applications of superhydrophobic, superomniphobic and non-textured, low surface energy coatings and films in reducing the adhesion of a low surface tension seed dressing to stainless steel. We characterized the wettability of our coatings with contact angle measurements and conducted experiments simulating the seed treatment process. We evaluated our coatings based on their reduction in seed dressing adhesion compared to stainless steel and mechanical durability to seed abrasion. Based on our results, the superhydrophobic coatings were ineffective at repelling the seed dressing and although superomniphobic coatings have great potential in reducing the adhesion of the seed dressing, they were not suitable for heavy abrasion applications due to their poor mechanical durability. A non-textured, low surface energy film was the best solution due to its reduced seed dressing adhesion along with its great mechanical durability. Our results provide new insights into methods to reduce liquid adhesion for beverage manufacturing, fuel transportation and pharmaceutical companies.

4.1.2 Literature Review

For a non-textured, non-reactive surface, the equilibrium work of adhesion, W_e between a liquid drop and solid surface can be calculated based on free energies of interfacial areas and the Young-Dupre equation[55] as:

$$W_e = \gamma_{LV}(1+\cos\theta) \tag{4.1}$$

Where θ is the equilibrium (Young's) contact angle and γ_{LV} is the liquid surface tension. The equilibrium work of adhesion assumes an ideal homogeneous, perfectly smooth surface. In practical applications, the work of adhesion is governed by the receding contact angle (minimum contact angle that a liquid droplet displays on a solid surface). So, the practical work of adhesion, W_p:[55]

$$W_p = \gamma_{LV}(1+\cos\theta_{rec}) \tag{4.2}$$

Where θ_{rec} is the receding contact angle of the liquid on the solid. In order to reduce the work of adhesion, the receding contact angle should be maximized.

The wettability of a liquid on a solid surface can be characterized by the contact angle. As mentioned in chapter 2 a low surface tension liquid typically has lower contact angle than a high surface tension liquid on the same solid surface. A surface with contact angle > 90° for water (γ_{LV} = 72 mN m^{-1}) is considered to be hydrophobic and a surface with contact angle >90° for both high (e.g., water) and low (e.g., oils) surface tension liquids is considered to be omniphobic. Typically, for a given liquid, a low γ_{SV} results in higher contact angles compared to a high γ_{SV}.[3,7,8] However, based on equation 4.2, the practical work of adhesion is a function of the receding contact angle. A more homogeneous surface (physically and chemically) of a given material will typically have a higher receding contact angle than a less homogeneous surface. Therefore, a non-textured, low solid surface energy film will have high advancing contact angles due to its low

surface energy and high receding contact angles due to its physical homogeneity (non-textured). The high contact angles and low contact angle hysteresis result in low liquid adhesion on the film.

The highest observed water contact angle on even the lowest solid surface energy non-textured surface is $\theta \approx 130°$.[9] Higher contact angles for water and oil can be achieved with textured surfaces.[10,11] When a liquid droplet contacts a textured surface, it displays the apparent contact angle θ^* and adopts one of the two possible states – Wenzel[12] state or Cassie-Baxter[13] state. In the Wenzel state, the liquid penetrates the texture and wets the surface completely. In the Cassie-Baxter state, air pockets are trapped between the surface and the liquid; therefore, the liquid contacts both air and solid. The Cassie-Baxter state is preferred for designing superhydrophobic and superomniphobic surfaces[10,14,18-20] because the air pockets reduce the solid-liquid contact area and result in high apparent advancing contact angles θ^*_{adv}, high apparent receding contact angles θ^*_{rec} and low contact angle hysteresis. A superomniphobic surface requires a specific type of texture called re-entrant (see chapter 2).[21-23] The re-entrant texture allows low surface tension liquids to adopt the Cassie state on the surface.

A surface is considered to be superhydrophobic when apparent contact angle > 150° and contact angle hysteresis is low for water[3,7,8,15,16] and superomniphobic when apparent contact angle >150° and contact angle hysteresis is low for virtually all liquids.[24-26] If a seed dressing droplet adopts the Cassie-Baxter state on a superhydrophobic or superomniphobic surface, it will display a high apparent receding contact angle and result in low practical work of adhesion between the seed dressing and solid surface. Consequently, the seed dressing will not adhere to the surface.

4.2 Materials/Methods/Experiments

We fabricated superhydrophobic (see section 4.2.1) and superomniphobic (see section 4.2.3) coatings and employed commercially available non-textured, low surface energy films (see

section 4.2.4) to investigate the repellency and mechanical durability of our coatings and films in reducing seed dressing adhesion. Advancing and receding contact angles of the seed dressing (liquid at room temperature) were measured on all coatings and films and the liquid adhesion was measured on coatings and films by exposure to wet seeds simulating seed treatment conditions in a rotational abrader (see section 4.2.8).

4.2.1 Fabrication of Superhydrophobic Coatings

We fabricated superhydrophobic stainless steel 316 via spray coating carnauba wax (**Figure 4.2a**).[56] The spray coating process introduced sufficient texture (**Figure 4.2b)** and carnauba wax imparted low solid surface energy, yielding a superhydrophobic coating on stainless steel. We characterized the wettability of our superhydrophobic coatings using contact angle measurements of the seed dressing. Our superhydrophobic coatings display apparent advancing contact angle = 162° and receding contact angle = 159° for water.

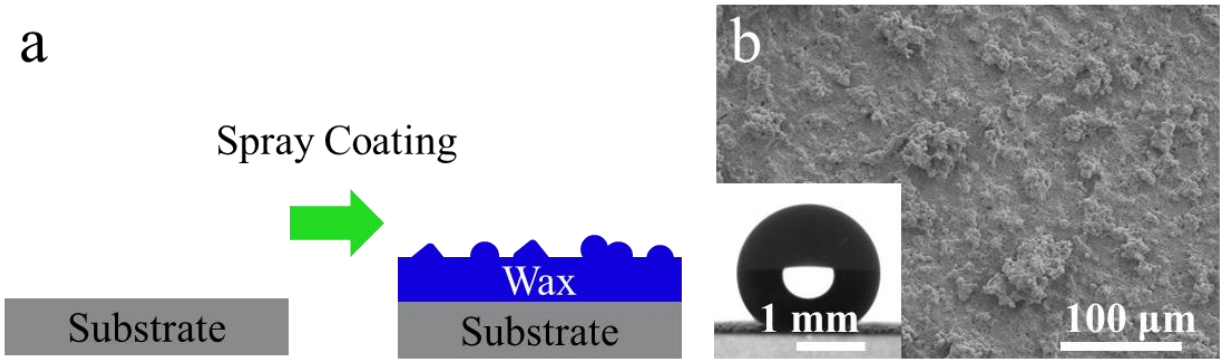

Figure 4.2. *a) Schematic of fabrication for superhydrophobic coatings. b) Scanning Electron Microscope (SEM) image of superhydrophobic coating with inset displaying water contact angle > 150°.*

4.2.2 Scanning Electron Microscope Images

Scanning electron microscope (SEM; JEOL-6500F) images were obtained at 10 kV and a working distance of 10 mm.

4.2.3 Fabrication of Superomniphobic Coatings

We fabricated our superomniphobic coatings via spin coating an adhesive (polyurethane) and subsequently spray coating a suspension of 10 nm fluorinated silica (F-SiO_2) particles in hexane[57] onto stainless steel. Stainless steel samples were cleaned with ethanol, thoroughly rinsed with deionized water and subsequently dried using nitrogen gas. An oil-based polyurethane (MINWAX®) was spin coated onto stainless steel using a G3P-8 spincoater (Specialty Coating Systems) at 500 rpm. Immediately after spin coating polyurethane (i.e., before polyurethane dried) a suspension of F-SiO_2 particles was spray coated. The suspension of F-SiO_2 particles was prepared via liquid phase silanization of 300 mg of fumed silica particles (diameter ~ 10 nm; Sigma-Aldrich) with 0.3 mL heptadecafluoro-1,1,2,2-tetrahydrodecyl)trichlorosilane (Gelest, a perfluorosilane) in 10 mL n-Hexane (Fisher) for three days to form a suspension of F-SiO_2 particles (**Figure 4.3a**). Over three days, the silane formed covalent bonds with silica particles and imparted low solid surface energy to the silica particles. The suspension of F-SiO_2 particles was spray coated on stainless steel at a pressure of 30 psi and the spray coater was held ~ 10 cm from the sample. Superomniphobicity was achieved once the coating completely covered the surface (**Figure 4.3b** and **c**). F-SiO_2 particles have low surface energy[24,25,32] and the spray coating process introduces re-entrant texture on the surface which makes the coating superomniphobic. The wettability of our superomniphobic coatings was characterized with contact angle measurements (see section 4.2.5) and the adhesion of our superomniphobic coatings was characterized by simulated seed dressing treatments (see section 4.2.8). Our superomniphobic coatings display apparent advancing contact

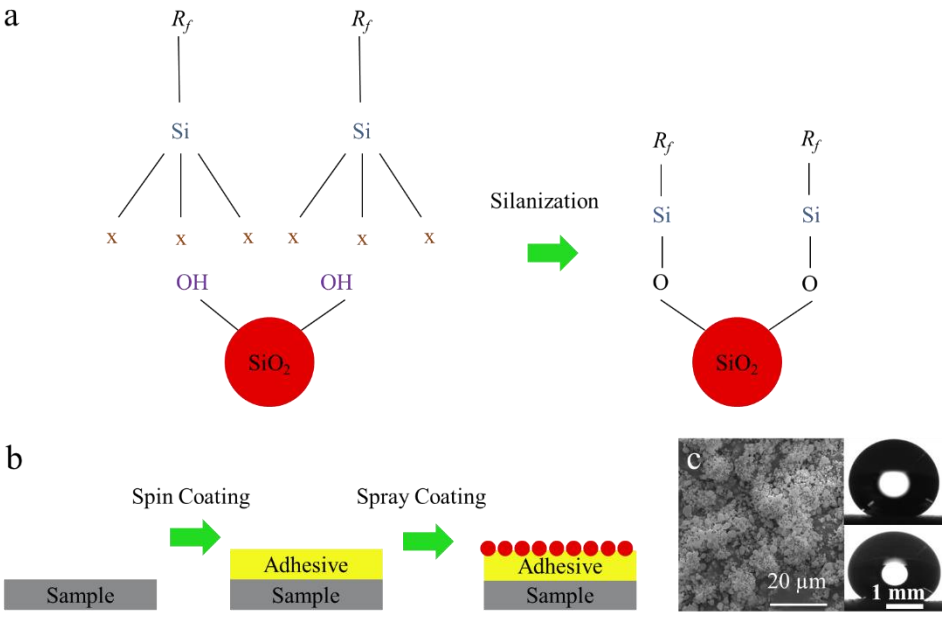

Figure 4.3. *a) Schematic of silanization for fumed silica particles. b) Schematic of fabrication for superomniphobic coatings. c) Scanning Electron Microscope (SEM) image of superomniphobic coating with insets displaying apparent contact angle >150° for water (top) and rapeseed oil (bottom).*

angle = 171° and receding contact angle = 162° for water and apparent advancing contact angle =160° and receding contact angle = 153° for rapeseed oil.

4.2.4 Non-Textured Low Surface Energy Films

Polyester, polypropylene, polyethylene and polytetrafluoroethylene non-textured films were obtained from McMaster. Contact angles were measured (see section 4.2.5) and the surface energy of all films was approximated using the Owens-Wendt approach (see section 4.2.6). The root mean square roughness of the films was measured using 3D optical profilometry (see section 4.2.7) and the seed dressing adhesion to the films was quantified by image analysis of coatings after adhesion tests (see section 4.2.8 and 4.2.9).

4.2.5 Contact Angle Measurements

Contact angle measurements of desired liquids were measured on superhydrophobic, superomniphobic and non-textured, low surface energy coatings and films using a Ramé-hart F260 Goniometer. Advancing and receding contact angles were measured by advancing or receding ~8

μL droplets on the coating or film using a syringe (Gilmont), respectively. At least five measurements were performed on each coating and film. The error in contact angle was ± 1°.

4.2.6 Estimation of Surface Energy

We estimated the surface energy using the Owens-Wendt approach.[41] According to this approach, the solid surface energy is the sum of contributions from two types of intermolecular forces at the surface:

$$\gamma_{SV} = \gamma_{SV}^{d} + \gamma_{SV}^{p} \tag{4.3}$$

Here, γ_{SV}^{d} is the component that accounts for the dispersive forces, while γ_{SV}^{p} is the component that accounts for the polar forces. Further, this approach postulates that:

$$\gamma_{SL} = \gamma_{SV} + \gamma_{LV} - 2\sqrt{\gamma_{SV}^{d}\gamma_{LV}^{d}} - 2\sqrt{\gamma_{SV}^{p}\gamma_{LV}^{p}} \tag{4.4}$$

Here, γ_{LV}^{d} and γ_{LV}^{p} are the dispersive and polar components of the liquid surface tension, respectively. Combining equations 2.1, 4.3 and 4.4 and recognizing that the polar component of liquid surface tension is zero ($\gamma_{LV}^{p} = 0$) for nonpolar liquids such as oils, the dispersive component of solid surface energy is given as:

$$\gamma_{SV}^{d} = \gamma_{LV}\left(\frac{1+\cos\theta}{2}\right)^{2} \tag{4.5}$$

Where γ_{LV} is the surface tension of a nonpolar liquid and θ is the equilibrium contact angle of the same nonpolar liquid on the solid surface. We used rapeseed oil (γ_{LV} = 35 mN m^{-1})[58] as the nonpolar liquid to estimate the dispersive component of solid surface energy. After determining the dispersive component γ_{SV}^{d}, combining equations 2.1, 4.3 and 4.4 for a polar liquid ($\gamma_{LV}^{p} \neq 0$), the polar component of the solid surface energy γ_{SV}^{p} is given as:

$$\gamma_{SV}^{p} = \frac{1}{\gamma_{LV}^{p}}\left[\frac{\gamma_{LV}(1+\cos\theta)}{2} - \sqrt{\gamma_{SV}^{d}\gamma_{LV}^{d}}\right]^2 \quad (4.6)$$

Where γ_{LV} is the surface tension of a polar liquid and θ is the equilibrium contact angle for the same polar liquid on the solid surface. We used water (γ_{LV}^{d} = 21.1 mN m^{-1} and γ_{LV}^{p} = 51.0 mN m^{-1}) as the polar liquid to estimate γ_{SV}^{p}. **Table 4.1** summarizes the solid surface energy values estimated by the Owens-Wendt approach. The advancing contact angle was used to approximate Young's contact angle.[42]

Table 4.1. Estimated Total Surface Energy for Non-Textured Films

Material	$\theta_{adv,water}$ (°)	$\theta_{adv,rapeseed\_oil}$ (°)	γ_{SV} (mN m^{-1})
Polyester	70	29	41
Polyethylene	98	33	31
Polypropylene	110	44	26
Polytetrafluoroethylene	112	60	20

4.2.7 Roughness Measurements

The root mean square roughness R_{rms} of the non-textured, low surface energy films was measured using an optical profilometer (Zygo Zescope). At least five measurements were performed at different locations on each film.

4.2.8 Seed Dressing Adhesion and Durability Testing

In order to simulate a seed treatment facility, we mounted samples along the interior of a 3.5-gal rotational abrader and added 400 mL of wet shell corn (40 mL of seed dressing). Shell corn was selected due to its hardness, sharp edges and tumbling nature. The abrader rotated axially, allowing the wet shell corn to tumble over the samples for 1 hr. (**Figure 4.4a** and **b**). Seed dressing adhesion was measured using image analysis and the durability of our samples was measured using root mean square roughness to quantify the physical inhomogeneity of our films.

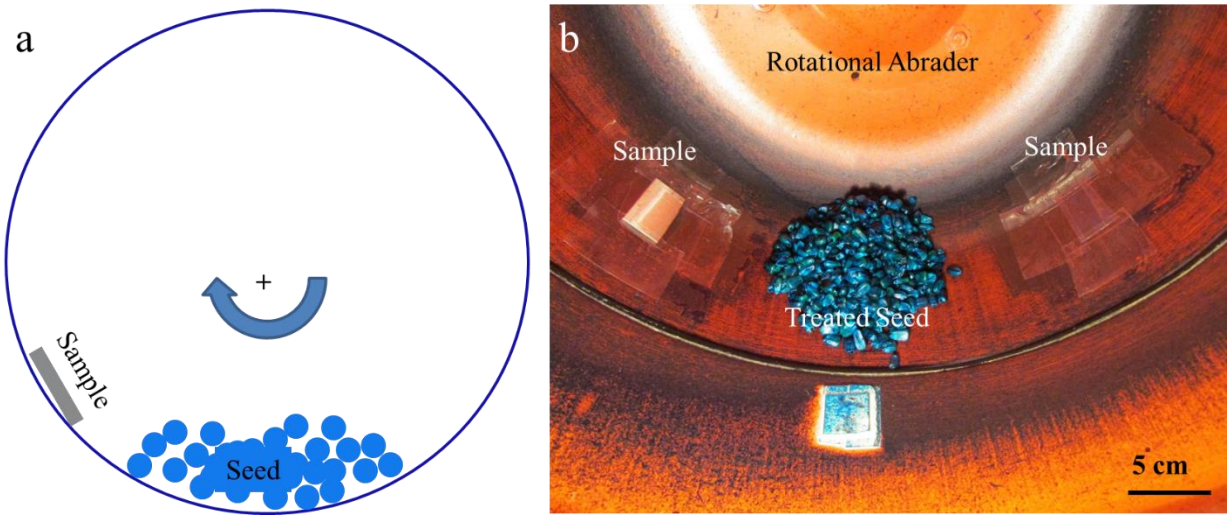

Figure 4.4. *a) Schematic of rotational abrader testing setup using treated seeds b) Image of liquid adhesion testing in rotational abrader.*

4.2.9 Image Analysis

We quantified the reduction in liquid adhesion for different samples in comparison to stainless steel by measuring the area fraction discolored, A_d on a sample after 1 hr. of tumbling with wet shell corn (see section 4.2.8). The seed dressing was dark blue which made the discolored area easy to distinguish. We measured the area fraction discolored by capturing optical images of the coatings after exposure to wet shell corn with a handheld camera (Canon, **Figure 4.5a**) under the same lighting conditions for all samples. A threshold was applied to the images using ImageJ (**Figure 4.5b**) and the area % that was discolored (from the seed dressing) was measured using ImageJ area fraction tool. More seed dressing coverage on the surface resulted in higher area

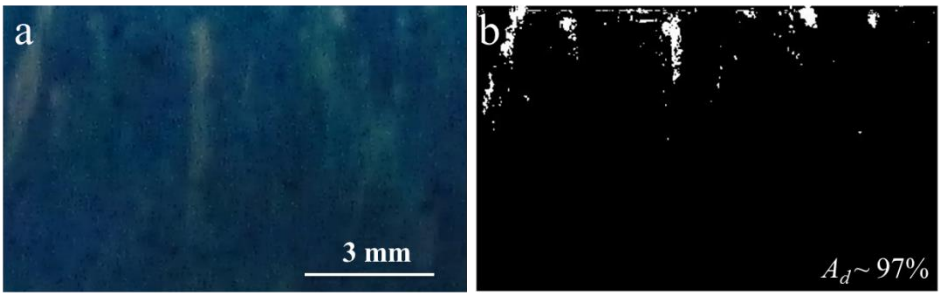

Figure 4.5. *a and b) Control stainless-steel original and post image processing image, respectively.*

fraction discolored, therefore the area fraction discolored was used as a representation of the seed dressing adhesion to the surface. On the stainless-steel control, A_d ~ 97%.

4.3 Results and Discussion

4.3.1 Performance of Superhydrophobic Coatings

We characterized the wettability of our superhydrophobic coatings with contact angle measurements of the seed dressing. Our superhydrophobic coatings had apparent receding contact angles <10° (due to the seed dressing adopting the Wenzel state (**Figure 4.6**). The seed dressing entered the Wenzel state on the superhydrophobic coating due to its low surface tension (γ_{LV} ~ 33 mN m^{-1}). Based on equation 4.2, extremely low apparent receding contact angles yield very high practical work of adhesion. We did not measure the liquid adhesion on our superhydrophobic coatings because the seed dressing droplet adopted the Wenzel state and displayed very low apparent receding contact angles. Therefore, our superhydrophobic coatings are not effective at reducing the adhesion of seed dressing to stainless steel.

Figure 4.6. *Seed dressing in Wenzel state on our superhydrophobic coating.*

4.3.2 Performance of Superomniphobic Coatings

A seed dressing droplet adopts the Cassie-Baxter state when placed on our superomniphobic coating and displays high receding contact angles. We measured the seed dressing adhesion of our superomniphobic coatings and the coatings were completely discolored after the adhesion test (**Figure 4.7a** and **b**).

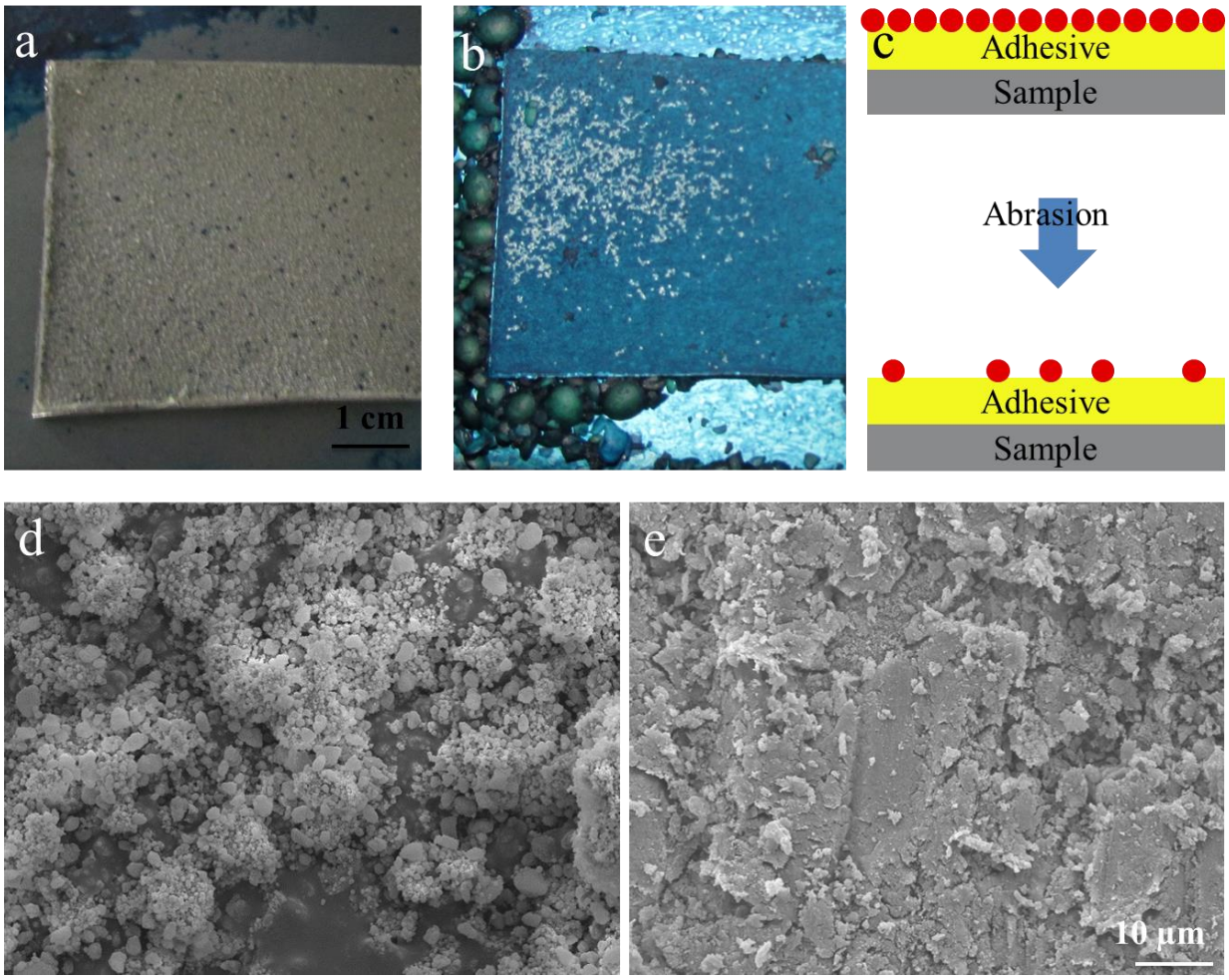

Figure 4.7. *a and b) Superomniphobic coating before and after 1 hr. of adhesion testing, respectively. c) Schematic of loss of re-entrant texture during abrasion. d and e) SEM image of before and after adhesion testing, respectively. The re-entrant texture in d is significantly damaged in e and the samples no longer have sufficient re-entrant texture to repel the seed dressing.*

In order to understand the mechanism of failure, SEM images of superomniphobic coatings before and after the abrasion test were taken. The mechanism of failure was determined to be removal of the textured coating due to the abrasion of seeds on the surface. The microscale texture

for a superomniphobic coating needs to have re-entrant texture (see section 2.3). F-SiO_2 particles spray coated onto the adhesive layer impart re-entrant texture on the surface (see **Figure 4.7c** and **d**). After abrasion, the re-entrant texture was damaged (**Figure 4.7e**) and the seed dressing adopted the Wenzel state on coatings resulting in a low apparent receding contact angle. The low apparent receding contact angle resulted in high practical work of adhesion and the seed dressing adhered to our superomniphobic coatings (A_d ~ 98%). Therefore, our superomniphobic coatings are not effective at reducing the adhesion of seed dressing to stainless steel.

4.3.3 Performance of Non-Textured, Low Surface Energy Films

We measured the root mean square roughness, R_{rms} of all non-textured films (**Table 4.2**) using optical profilometry (see section 4.2.7).

Table 4.2. RMS roughness of Non-Textured Films

Material	R_{rms} (nm)
Polyester	56 ± 23
Polyethylene	340 ± 30
Polypropylene	210 ± 48
Polytetrafluoroethylene	160 ± 59

We estimated the solid surface energy of our non-textured films polyester, polyethylene, polypropylene and polytetrafluoroethylene films using the Owens-Wendt method (see section 4.2.6) and measured the seed dressing contact angles on the films. As expected from equation 2.1, films with lower surface energy have higher advancing and receding contact angles compared to higher surface energy films (**Figure 4.8**).

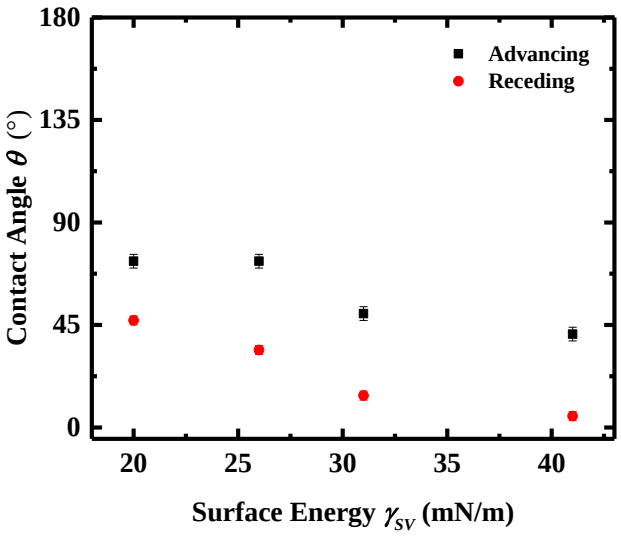

Figure 4.8. *Advancing and receding contact angles of seed dressing on non-textured films, polyester (41 mN m^{-1}), polyethylene (31 mN m^{-1}), polypropylene (26 mN m^{-1}), polytetrafluoroethylene (20 mN m^{-1}). Contact angles increase with decreasing surface energy.*

The seed dressing adhesion to our non-textured films was compared to stainless steel and the percent reduction in adhesion was quantified using image analysis (see sections 4.2.8 and 4.2.9). Lower surface energy films had a lower area fraction discolored than higher surface energy films (**Figure 4.9a**) which confirms higher receding contact angle results in lower adhesion based on equation 4.2. Polyester (41 mN m^{-1}) displayed seed dressing adhesion similar to stainless steel (A_d ~ 99%, **Figure 4.9b**). Polytetrafluoroethylene (20 mN m^{-1}) displayed ~80% reduction in seed dressing adhesion compared to stainless steel (A_d ~ 14%, see **Figure 4.9c**). Based on these results, a non-textured, low surface energy film attached to stainless steel will reduce liquid adhesion and

seed dressing buildup on the surface which has the potential to dramatically reduce cleaning costs in a seed treatment facility.

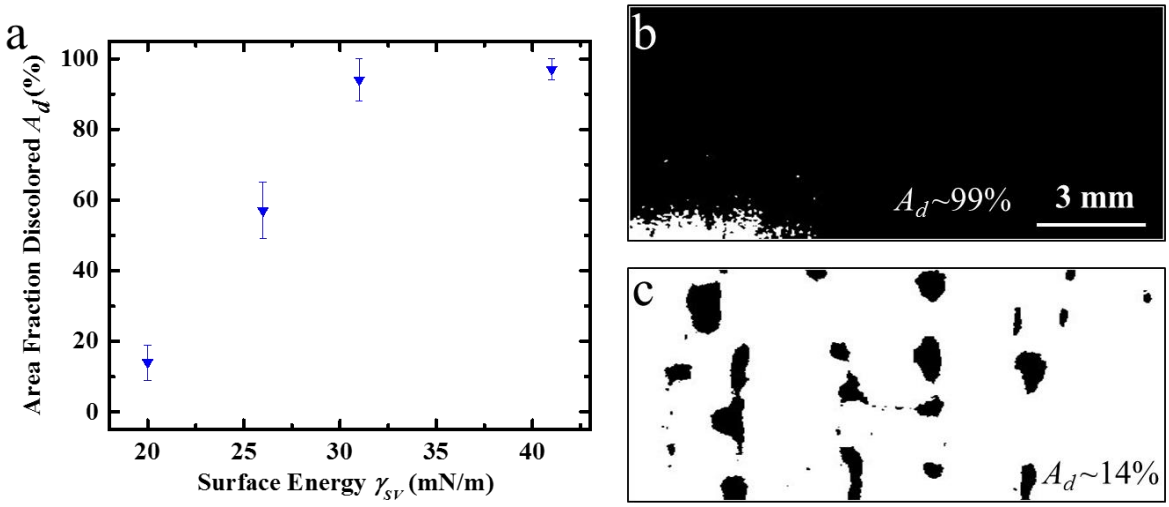

Figure 4.9. *a) Area fraction discolored on non-textured films with varying surface energy (stainless steel control: A_d ~ 97%). Polyester (41 mN m^{-1}), polyethylene (31 mN m^{-1}), polypropylene (26 mN m^{-1}), polytetrafluoroethylene (20 mN m^{-1}). Discoloration decreases with decreasing surface energy. b and c) Post processed image of 41 mN m^{-1} film and 20 mN m^{-1} film after exposure, respectively.*

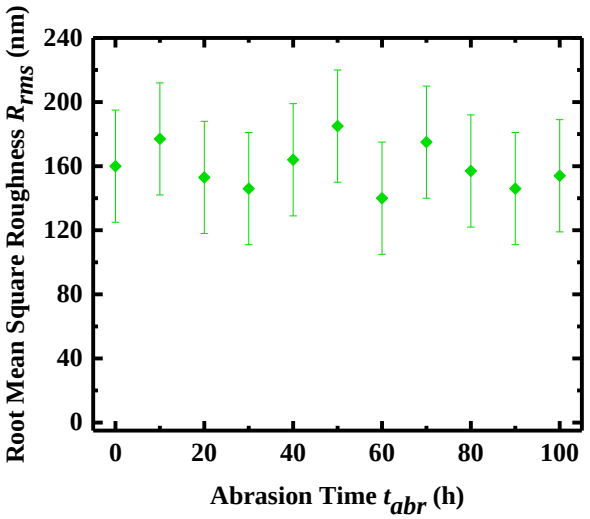

Figure 4.10. *Root mean square roughness of polytetrafluoroethylene (20 mN m^{-1}) at varying times of abrasion. The roughness does not change significantly even after 100 hours of abrasion.*

The mechanical durability of the best film (polytetrafluoroethylene) was tested using 5 L dry shell corn abrasion in a rotational abrader (**Figure 4.10)** and the root mean square roughness values did not increase significantly after 100 hours of abrasion. This indicates that the non-textured films will retain their reduced liquid adhesion over a long period of use in a seed treatment facility.

4.4 Conclusions

In conclusion, we studied the application of superhydrophobic, superomniphobic and non-textured, low surface energy coatings and films in reducing the adhesion of a low surface tension seed dressing to solid surfaces. We conducted experiments simulating a seed treatment process and evaluated our coatings and films based on their reduced seed dressing adhesion and their mechanical durability to seed abrasion. Based on our results, our superhydrophobic coating did not repel the low surface tension seed dressing and although superomniphobic coatings have great potential in reducing the adhesion of seed dressing, they were not suitable for heavy abrasion seed treatment application due to their poor mechanical durability. A non-textured, low surface energy film was the best solution due to its capability to reduce seed dressing adhesion and its great mechanical durability. We envision our results will have potential applications in reducing liquid adhesion for beverage manufacturing companies, fuel transportation companies and pharmaceutical companies.

5 SUPERHYDROPHOBIC SURFACES FOR REDUCING CONTACT TIME

5.1 Literature Review

5.1.1 Contact Time

When a liquid droplet impacts a superhydrophobic surface, the droplet typically rebounds from the surface and the amount of time that the droplet is in contact with the solid surface is defined as the contact time *t*. The contact time is an important factor in heat transfer between a liquid droplet and solid surface because energy transfer between the droplet and solid only occurs during the contact time. Consider a droplet impacting a cold solid (e.g., airplane wing), if the contact time is sufficiently long, the droplet temperature will reduce far enough to freeze on the solid and form ice. However, if the contact time is short, the droplet will not lose enough energy to freeze and will bounce off from the surface. The contact time is proportional directly to the inertia and inversely to the capillarity of the droplet as:[59]

$$t \sim \sqrt{\frac{\rho r_d^3}{\gamma_{LV}}} \tag{5.1}$$

Where, r_d is the droplet radius, ρ and γ_{LV} are the droplet's density and surface tension, respectively. It is also influenced by the internal dissipation and surface-liquid adhesion.[60] Lv *et al.* (2016)

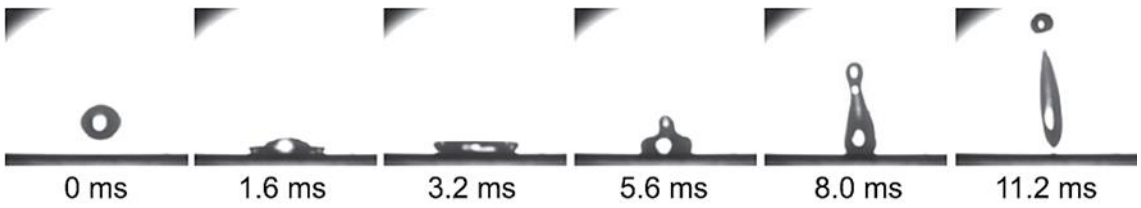

Figure 5.1. *Snapshots of a 4 μL droplet impacting on a superhydrophobic surface at an impact velocity of 1.4 m* s^{-1}.[4]

studied the contact time of a water droplet impacting a superhydrophobic surface.[4] They showed that once the droplet impacts the superhydrophobic surface, it spreads to the maximum spreading

configuration, then recoils on the surface and eventually detaches and bounces back from the surface (**Figure 5.1**). Therefore, the contact time t on a superhydrophobic surface can be defined as the sum of two time spans, the spreading time t_s (e.g., $t < 3.2$ ms) and the recoil time t_r (e.g., $t > 3.2$ ms) as.[61]

$$t = t_s + t_r \tag{5.2}$$

Among the many characteristics of superhydrophobic surfaces, the capability to reduce the contact time of water over a wide range of impact velocities has been an area of study in recent years.[2,4,5,60-64] Further reductions in contact time enable a wider range of anti-icing applications and improve the performance of superhydrophobic surfaces in anti-icing applications.

5.1.2 Methods to Reduce Contact Time

Thus far, significant attempts (experimental and numerical) have been devoted to reduce the contact time through altering the hydrodynamics of the droplet when it is in contact with super-repellent surfaces (**Figure 5.2**).[5] For example, Bird *et al.* (2013) showed that a small macroscale ridge on a superhydrophobic surface can significantly reduce the contact time relative to a non-macroscale textured superhydrophobic surface due to center-assisted variation of the

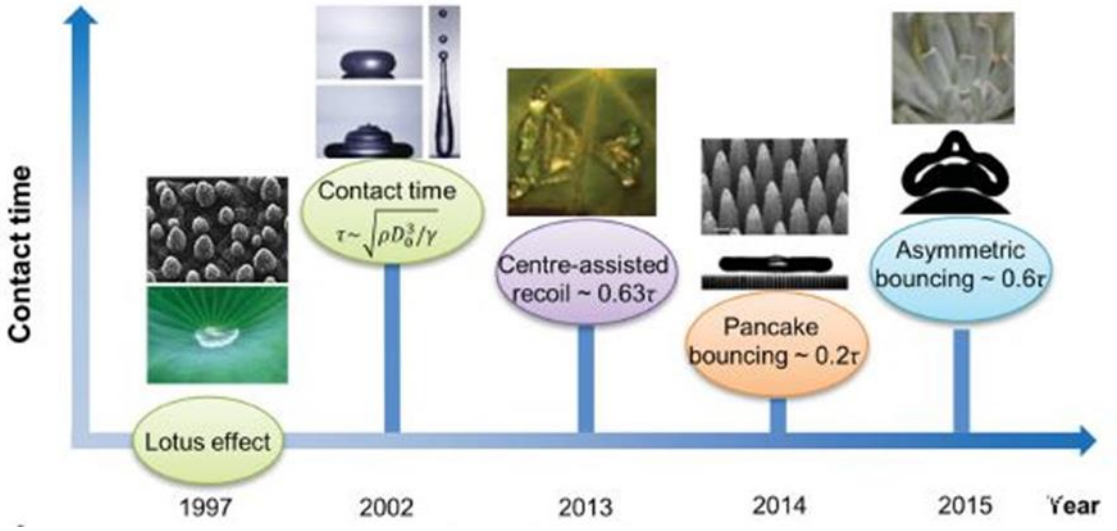

Figure 5.2. *Strategies for contact time reduction.*[5]

hydrodynamics of the droplet during its recoil (**Figure 5.2**).[62] They demonstrated that when a droplet impacts the macrotexture of a superhydrophobic surface, it spreads on the surface (t_s does not change noticeably) and then detaches from the surface (without recoiling on the surface) and recoils in the air (**Figure 5.3**). Leveraging the macro-texture on the superhydrophobic surface, they could almost eliminate the recoil time t_r which led to ~ 40% reduction in contact time (**Figure 5.3**).

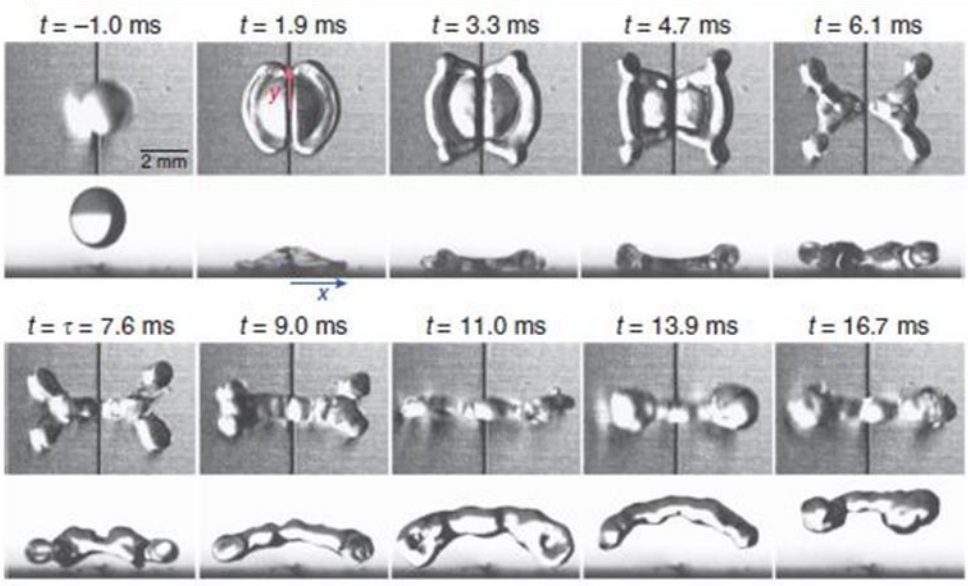

Figure 5.3. *Droplet volume reconfiguration for reducing contact time.*[2]

Liu *et al.* (2014) demonstrated pancake bouncing where the droplet lifts off the surface without recoiling therefore significantly reducing contact time based on equation 5.2 (**Figure 5.2)**. The pancake effect is due to the conversion of capillary energy stored in the deformed liquid into upward motion adequate to lift the drop.[64] In another attempt, Liu *et al*. (2015) showed asymmetric bouncing on surfaces with curvature greater than the impacting droplet radius (**Figure 5.2)**.[63] Shen *et al.* (2015) showed a reduction in contact time utilizing multiple intersecting ridges in Y and cross shaped patterns to reconfigure droplet volume into smaller subunits.[61]

Gauthier *et al*. (2015) extended the work conducted by Bird *et al.* and studied the effect of impact velocity on contact time of a droplet on a superhydrophobic surface possessing a

macrotexture.[2] They demonstrated a step wise decrease in contact time at intermediate and high impact velocities on a macrotexture superhydrophobic surface. They explained the step wise reduction is due to the formation of water droplet subunits which by definition have smaller volumes than the original droplet. Smaller droplets have lower r_d and thus inertia which results in reduced contact time based on equation 5.1. These papers demonstrate that hemispherical ridges and ridge patterns are effective in reducing contact time with macroscale textures. While curved surfaces have been extensively studied in relation to contact time, the effect of ridge height with triangular ridges has not been investigated. In this work, we investigated the effect of ridge height on contact time of macroscale textured superhydrophobic surfaces.

5.2 Materials/Methods/Experiments

5.2.1 Macroscale Texture

Aluminum (Al) surfaces were machined using a belt grinder to fabricate an Al ridge with included angle (e.g., ridge angle) $\alpha = 90°$ and height > 2 mm. We selected a ridge angle of 90° to use in our preliminary work. We investigated the effect of ridge height for a ridge angle $\alpha = 90°$ over a wide range of weber number (see section 5.2.2) on our superhydrophobic coatings (see chapter 3). Two other Al surfaces (flat surfaces) were chamfered at 45° to enable a smooth fit between the three pieces in the ridge system (**Figure 5.4a**). The flat surfaces were placed horizontally at different heights along the ridge to fabricate varying ridge heights h_r (**Figure 5.4a** and **b**). Al surfaces with and without macroscale texture were spray coated with our superhydrophobic coating (see section 3.2.1 for experimental details) with carnauba wax at $\rho_s \sim 0.6$ mg mL^{-1}.

5.2.2 Experimental Definitions

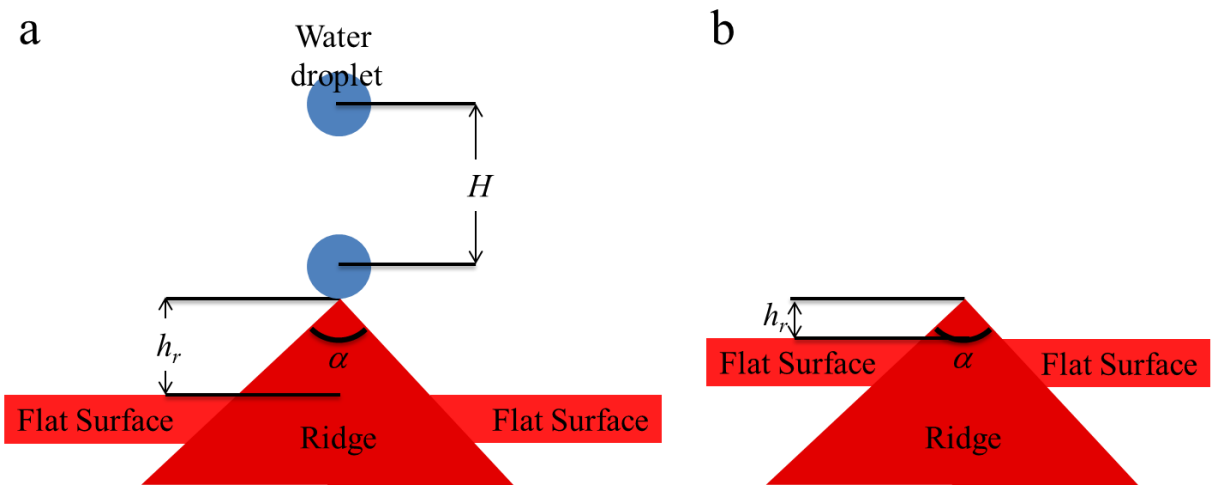

Figure 5.4. *a) Schematic of ridge setup and definition of ridge height h_r, ridge angle α and center to center height H (between droplet release point and droplet impact). b) Schematic of smaller ridge height compared to ridge in a.*

The impact of water droplets at different velocities was captured using a Photron Fastcam SA3 camera at 3000 frames per second. The movies were analyzed using Photron FASTCAM Viewer (PFV) and the length of time that the droplet was visually in contact with the Al surface (contact time *t*) was determined. The impact velocity of water droplets on all surfaces was systematically varied by releasing water droplets at different heights *H* above the ridge. The droplet release height *H* was defined as the center to center distance between droplet release and droplet impact on the ridge (**Figure 5.4a**). The impact velocity was approximated as:

$$v \sim \sqrt{2gH} \tag{5.3}$$

Where g is the gravitational acceleration due to gravity in m s^{-2} and H is the center to center distance in m. Weber number (*We)* was calculated as:

$$We = \frac{\rho v^2 r_d}{\gamma_{LV}} \tag{5.4}$$

Where ρ and γ_{LV} are the density and surface tension of water, respectively. The center to center distance was measured using PFV for $We < 7$ and using a ruler for $We > 7$ (due to constraints on

the camera field of view). The droplet radius was held constant at r_d = 1.35 ± 0.02 mm using a syringe pump (GenieTouch^{TM}). At least 3 different experiments were conducted for each *We*.

For practical applications, the macroscale texture is an improvement only if $t < t_{flat}$ where t_{flat} is the contact time on a superhydrophobic surface without macroscale texture. Therefore, we report our results in terms of a normalized contact time ($t^* = t/t_{flat}$). On our superhydrophobic Al surfaces without macroscale texture, t_{flat} = 15.2 ± 1 ms.

5.3 Results and Discussion

We systematically evaluated the effect of ridge height on normalized contact time as a function of *We* (**Figure 5.5**). According to our preliminary results (**Figure 5.5**), we can define four different regimes of *We* number based on the hydrodynamics of the droplet. For *We* < 2, the

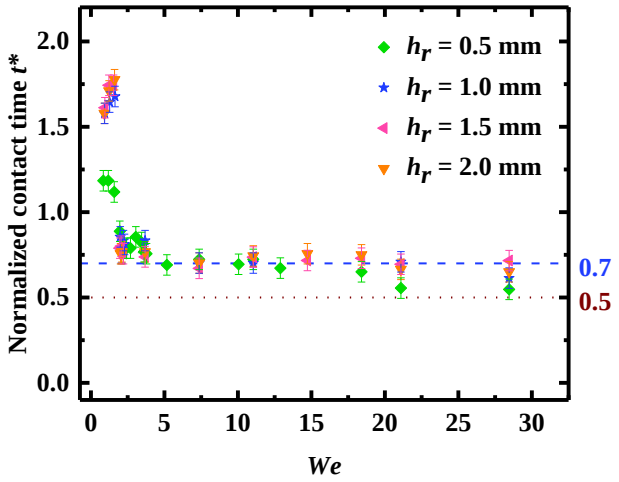

Figure 5.5. *Plot of normalized contact time t* as a function of We for varying ridge heights with α = 90°. Blue and brown lines denote predicted t* for 2 and 4 subunit reconfigurations, respectively.*

droplet spreads and recoils on the surface similar to a superhydrophobic surface without a macroscale texture (**Figure 5.6a-c**). However, the presence of the ridge causes an extra term in the contact time (i.e., $t = t_s + t_r + 2t_{ridge}$). t_{ridge} is defined as the time between when the droplet hits the tip of the ridge and the time it hits the bottom flat surface. t_{ridge} is always greater than zero which

results in $t^* > 1$ for h_r = 0.5, 1.0, 1.5 and 2.0 mm ridges at $We < 2$. As expected, at low We (i.e., We < 2), increasing h_r and thereby the travel distance of the droplet on the ridge results in further

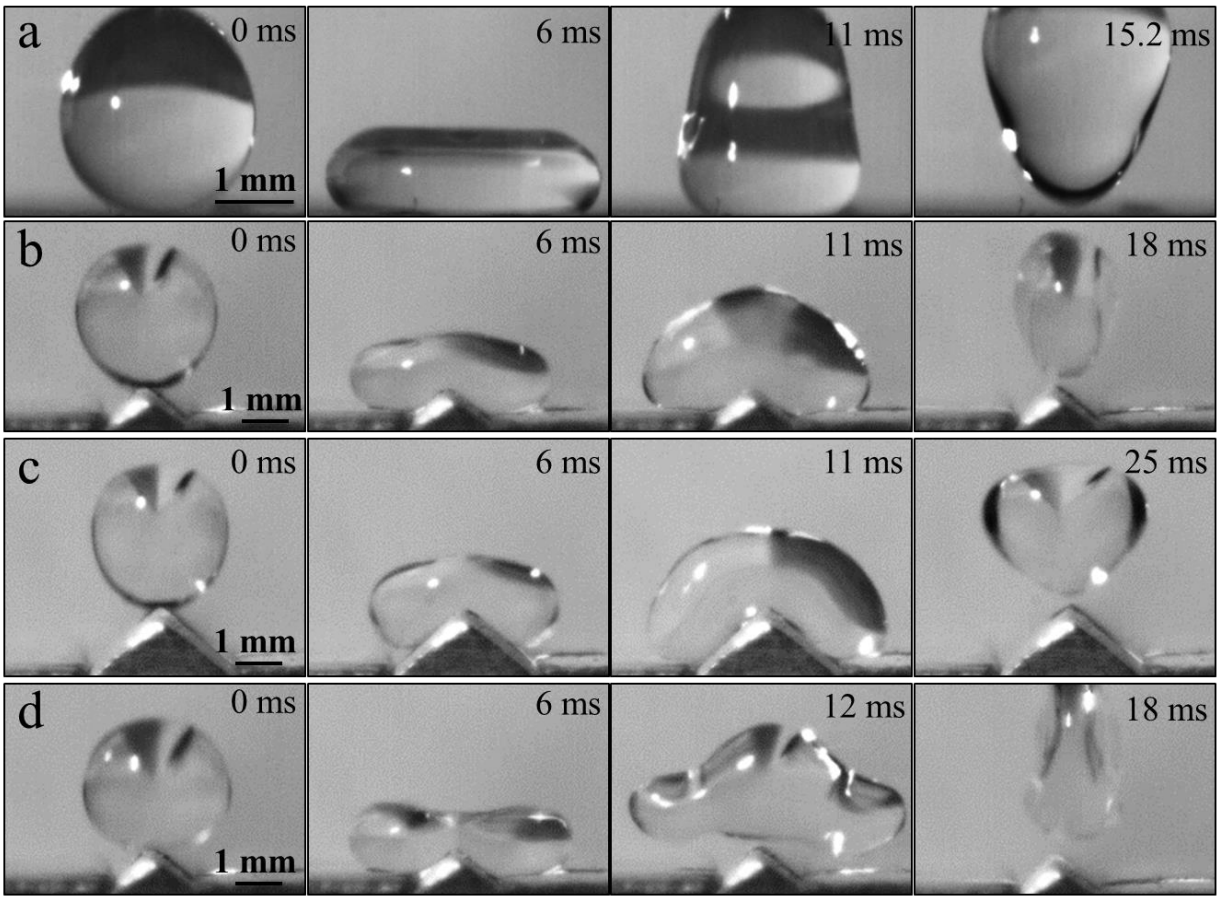

Figure 5.6. *a) Snapshots of droplet impact for We = 1.2 on superhydrophobic coating without macroscale texture. b and c) Snapshots of droplet impact for We = 1.2 (h_r = 0.5 mm, α = 90°, t^* = 1.2) and (h_r = 1.0 mm, α = 90°, t^* = 1.6), respectively. The droplet spreads and recoils on the surface before detaching from the top of the ridge. $t^* > 1$ due to the time spent spreading and recoiling on the ridge (t_{ridge}). d) Snapshots of droplet impact for We = 2.4 (h_r = 0.5 mm, α = 90°, t^* = 0.79). The droplet detaches from the surface before recoiling resulting in a reduction in normalized contact time.*

increase of t^* (**Figure 5.6b** and **c**). For $h_r > 1.0$ mm, t^* does not increase significantly because the droplet no longer hits the bottom surface for $We < 2$.

Now, let us consider the 2nd regime of We number ($2 \leq We < 7$). In this regime, the droplet spreads on the surface and then detaches without recoiling on the surface (**Figure 5.6d**). This significantly reduces t_r and results in $t^* < 1$ for $h_r = 0.5$, 1.0, 1.5 and 2.0 mm ($t^* \sim 0.8$).

In the 3rd regime of We ($7 \leq We < 22$), t^* is further reduced due to reconfiguration of the droplet into 2 subunits (**Figure 5.7a** and **b**). These subunits by definition have smaller volumes

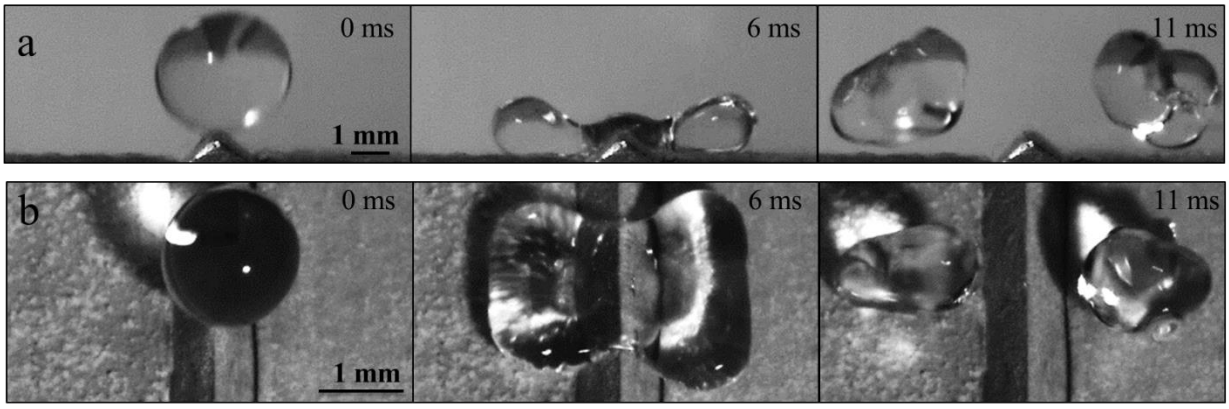

Figure 5.7. *Snapshots of droplet impact for We ~ 7, (h_r = 0.5 mm, α = 90°, t* = 0.72). a and b) Side view and top view, respectively. The droplet reconfigures into 2 subunits during impact.*

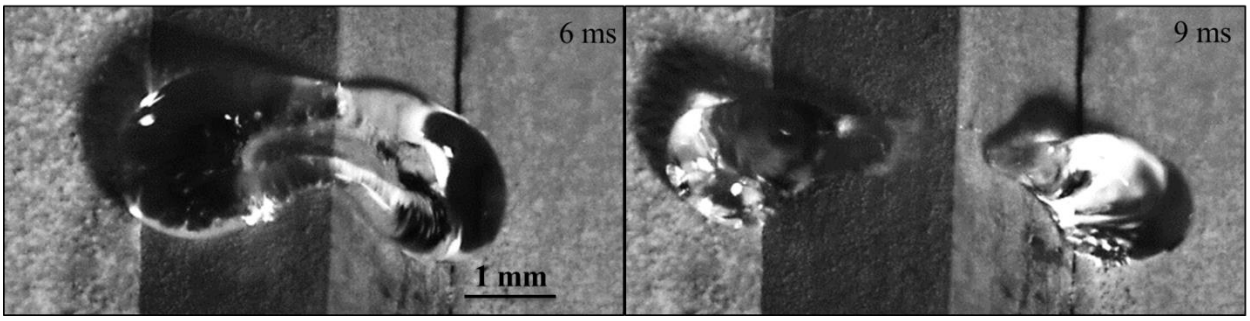

Figure 5.8. *Snapshots of droplet impact for We ~ 7 (h_r = 2.0 mm, α = 90°, t* = 0.72). The droplet reconfigures into 2 subunits.*

and radii than the original droplet and have lower contact times as evident based on equation 5.1.[2] Gauthier *et al*. demonstrated that the contact time in this regime can be scaled as:[2]

$$t^* = \frac{1}{\sqrt{N}} \tag{5.5}$$

Where N is the number of subunits formed during impact. Our results (**Figure 5.5**) indicate that t^* reduced to ~ 0.72 in this regime which is very close to 0.707 predicted based on equation 5.5. Despite some differences caused by different ridge heights (**Figure 5.7b** and **Figure 5.8**) two subunits are formed on all ridges in this regime resulting in similar contact times.

In the 4th regime of *We* ($22 \leq We < 30$), t^* is further reduced for $h_r = 0.5$ mm but not for $h_r > 0.5$ mm. The reduction in t^* for $h_r = 0.5$ mm is due to the reconfiguration of the droplet into 4 subunits (**Figure 5.9**). The predicted $t^* = 0.5$ value (based on equation 5.5) is similar to the experimental $t^* \sim 0.55$. However, $h_r > 0.5$ mm do not display a reduction in t^* because the droplet forms 2 subunits (**Figure 5.10)** as was observed in regime 3. The droplet forms 2 subunits on $h_r \geq$

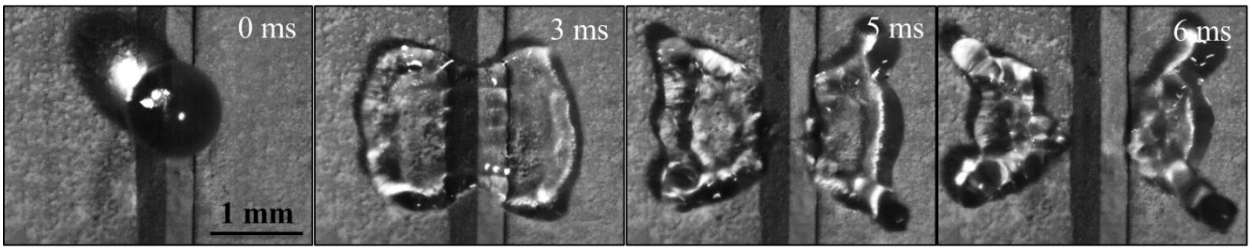

Figure 5.9. *Snapshots of droplet impact at We = 22 (h_r = 0.5 mm, α = 90°, $t^* \sim 0.55$). The droplet reconfigures into 4 lobes resulting in $t^* \sim 0.5$.*

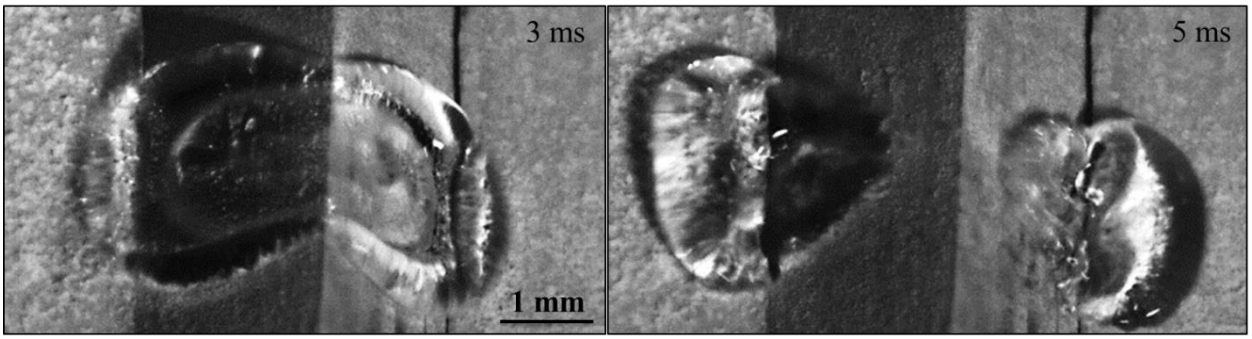

Figure 5.10. *Snapshots of droplet impact at We = 22 (h_r = 2.0 mm, α = 90°, $t^* \sim 0.68$). The droplet reconfigures into 2 lobes.*

1.0 mm for $We < 28$ because the droplet rapidly detaches from the top of the ridge due to the similar length scales of r_d and h_r when $h_r \geq 1.0$ mm. This detachment at the ridge removes the force resisting motion perpendicular to the ridge and allows the 2 subunits to freely move perpendicular to the ridge.

5.4 Conclusions

In this work, we fabricated superhydrophobic surfaces with varying heights of macroscale texture to investigate the influence of ridge height on water droplet contact time. We present four *We* number regimes and demonstrate that $t^* < 1$ for $We > 2$. For $We < 2$, $t^* > 1$ due to the time required to travel along the ridge, t_{ridge}. For $2 \leq We < 7$, $t^* < 1$ due to the droplet detaching before recoil reducing t_r. For $7 \leq We < 22$, $t^* \sim 0.7$ due to the reconfiguration of the droplet into 2 subunits which individually have lower contact time because of the scaling of contact time with respect to droplet radius. For $22 \leq We < 28$, $h_r = 0.5$ mm displays further reduction in t^* due to the droplet reconfiguring into 4 subunits. Ridges with $h_r = 1.0$, 1.5 and 2.0 mm continue to reconfigure into 2 subunits and do not display a significant reduction in t^*. Based on our results, $h_r = 0.5$ mm will typically display similar or lower t^* compared to $h_r = 1.0$, 1.5 and 2.0 mm over a wide range of *We*. We envision these findings will improve the design of macroscale textured superhydrophobic surfaces for anti-icing applications.

6 FUTURE WORK

6.1 Edible Superhydrophobic Coatings

This work presents a solution to reduce liquid waste but the most improvement would be from a durable coating that allows a container to be reused and applied to a variety of different surfaces for applications in medical, pharmaceutical and cosmetic industries. Once a durable superhydrophobic coating with edible materials is made, the possibilities in making clothes, kitchen utensils, pots and pans stain resistant are endless. The simplest method of fabricating a durable superhydrophobic coating would be to add an adhesive to the current fabrication method. The adhesive could improve the amount of wax that is coated on the surface (therefore reducing the amount of material required to achieve superhydrophobicity) but more importantly, the adhesive would help the wax withstand some mechanical abrasion.

The current spray-coating method works decently well for small-scale testing with easy-spraying materials. However, high-solids mixtures and mixtures with particles dispersed in solvents tend to clog the spray-guns and occasionally provide inconsistent surfaces. To ensure that coatings are repeatable, testing multiple coating methods with a single coating would ensure that anomalies are not being created by the spraying process. Use of an atomizer nozzle and rotating bed (with highly controlled height, pressure, and flow rate) could provide an easily repeatable coating method for testing. More precise control of coating parameters would improve potential interest in production scaling-up of the coating procedure for commercial applications.

6.2 Reducing Liquid Adhesion for Manufacturing Equipment

While the current state of superomniphobic coatings is not durable, further work should investigate different coating materials or mixtures to increase the hardness of the coating. A higher

receding contact angle reduces liquid adhesion, therefore a superomniphobic coating is the preferred ultra-low adhesion coating. The superomniphobic coating requires re-entrant texture and a harder base material in the coating could increase durability by increasing the energy necessary to damage the material. Another potential method to increase durability of the superomniphobic coating is to utilize the segregation of low surface-energy particles to the surface of a higher surface-energy matrix as highly adhesive materials tend to have higher surface energies. This would allow the adhesive and fluorinated particles to be spray coated at the same time potentially resulting in an improved bond between the adhesive and fluorinated particles. Also, using a ductile or low modulus adhesive could improve the durability of the coating by allowing the coating to "bend but not break".

A standard abrasion method for testing low adhesion films should be selected either with the use of a taber abrader (e.g., linear reciprocating abrasion) or internal fluid shear test using the seed dressing. This would significantly improve future testing methods for low adhesion films in seed treatment applications. In order to demonstrate real world application, a test film should be attached to the seed treatment hopper and the performance of the film should be recorded over a year with information such as the difference in seed dressing buildup on the film vs stainless steel and the agglomeration of seeds on the surface of the film and stainless steel.

6.3 Superhydrophobic Surfaces for Reducing Contact Time

While the effect of ridge height is a necessary step in understanding droplet impact on macroscale texture, the influence of ridge angle needs to be considered in future work. In addition, the effect of ridge height with different angles should be probed at the same time. Future experiments with simultaneous side and isometric views are recommended to enable specific correlations between observed hydrodynamics. In order to validate potential applications in the

aeronautics industry, further testing with $1000 < We < 5000$ should be performed on a robust superhydrophobic surface to determine if the reduction in contact time is possible at extremely high *We*. If potential contact time reduction exists, the macroscale texture could be used for anti-icing on airplanes. This would also require testing in durability and lift parameters with macroscale textured superhydrophobic surfaces.

7 REFERENCES

1 A K. Kota, Colorado State University 2015 Spring.

2 Gauthier, A.; Symon, S.; Clanet, C.; Quéré, D. Water impacting on superhydrophobic macrotextures. *Nat. Commun.* **2015**, *6*.

3 Kota, A. K.; Kwon, G.; Tuteja, A. The design and applications of superomniphobic surfaces. *NPG Asia Mater.* **2014**, *6*, e109.

4 Lv, C.; Hao, P.; Zhang, X.; He, F. Drop impact upon superhydrophobic surfaces with regular and hierarchical roughness. *Appl. Phys. Lett.* **2016**, *108*, 141602.

5 Hao, C.; Liu, Y.; Chen, X.; Li, J.; Zhang, M.; Zhao, Y.; Wang, Z.; Bioinspired interfacial materials with enhanced drop mobility: From fundamentals to multifunctional applications. *Small* **2016**, *12* (14), 1825-1839.

6 Young, T. An essay on the cohesion of fluids. *Philos. Trans. R. Soc.* **1805**, *95*, 65-87.

7 Kota, A. K.; Choi, W.; Tuteja, A. Superomniphobic surfaces: design and durability. *MRS Bull.* **2013**, *38*, 383-390.

8 Kota, A. K.; Mabry, J. M.; Tuteja, A. Superoleophobic surfaces: design criteria and recent studies. *Surf. Innovations*. **2013**, *1*, 71-83.

9 Genzer, J.; Efimenko, K. Creating Long-Lived Superhydrophobic Polymer Surfaces Through Mechanically Assembled Monolayers. *Science.* **2000**, *290*, 2130-2133.

10 Marmur, A. Wetting on hydrophobic rough surfaces: to be heterogeneous or not to be? *Langmuir*. **2003**, *19*, 8343-8348.

11 Öner, D.; McCarthy, T. J. Ultrahydrophobic surfaces. Effects of topography length scales on wettability. *Langmuir*. **2000**, *16*, 7777-7782.

12 Wenzel, R. N. Resistance of solid surfaces to wetting by water. *Ind. Eng. Chem.* **1936**, *28*, 988-994.

13 Cassie, A.; Baxter, S. Wettability of porous surfaces. *Trans. Faraday Soc.* **1944**, *40*, 546-551.

14 Patankar, N. A. On the modeling of hydrophobic contact angles on rough surfaces. *Langmuir*. **2003**, *19*, 1249-1253.

15 Kota, A. K.; Li, Y.; Mabry, J. M.; Tuteja, A. Hierarchically structured superoleophobic surfaces with ultralow contact angle hysteresis. *Adv. Mater.* **2012**, *24*, 5838-5843.

16 Lafuma, A.; Quéré, D. Superhydrophobic states. *Nat. Mater.* **2003**, *2*, 457-460.

17 Furmidge, C. Studies at phase interfaces. I. The sliding of liquid drops on solid surfaces and a theory for spray retention. *J. Colloid Sci.* **1962**, *17*, 309-324.

18 Herminghaus, S. Roughness-induced non-wetting. *EPL.* **2000**, *52*, 165.

19 Johnson Jr, R. E.; Dettre, R. H. Contact angle hysteresis. III. Study of an idealized heterogeneous surface. *J. Phys. Chem.* **1964**, *68*, 1744-1750.

20 Movafaghi, S.; Leszczak, V.; Wang, W.; Sorkin, J. A.; Dasi, L. P.; Popat, K. C.; Kota, A. K. Hemocompatibility of superhemophobic titania surfaces. *Adv. Healthcare Mater.* **2017**, *6*.

21 Marmur, A. From hygrophilic to superhygrophobic: theoretical conditions for making high-contact-angle surfaces from low-contact-angle materials. *Langmuir*. **2008**, *24*, 7573-7579.

22 Ahuja, A.; Taylor, J. A.; Lifton, V.; Sidorenko, A. A.; Salamon, T. R.; Lobaton, E. J.; Kolodner, P.; Krupenkin, T. N. Nanonails: A simple geometrical approach to electrically tunable superlyophobic surfaces. *Langmuir*. **2008**, *24*, 9-14.
23 Cao, L.; Price, T. P.; Weiss, M.; Gao, D. Super water-and oil-repellent surfaces on intrinsically hydrophilic and oleophilic porous silicon films. *Langmuir*. **2008**, *24*, 1640-1643.
24 Liu, K.; Tian, Y.; Jiang, L. Bio-inspired superoleophobic and smart materials: design, fabrication, and application. *Prog. Mater. Sci.* **2013**, *58*, 503-564.
25 Nishimoto, S.; Bhushan, B. Bioinspired self-cleaning surfaces with superhydrophobicity, superoleophobicity, and superhydrophilicity. *RSC Adv.* **2013**, *3*, 671-690.
26 Tuteja, A.; Choi, W.; Ma, M.; Mabry, J. M.; Mazzella, S. A.; Rutledge, G. C.; McKinley, G. H.; Cohen, R. E. Designing superoleophobic surfaces. *Science*. **2007**, *318*, 1618-1622.
27 Williams, H.; Wikstrom, F. Environmental Impact of Packaging And Food Losses in a Life Cycle Perspective: A Comparative Analysis of Five Food Items. *J. Cleaner Prod.* **2011**, *19*, 43-48.
28 Cheng, M. J.; Song, M. M.; Dong, H. Y.; Shi, F. Surface Adhesive Forces: A Metric Describing the Drag-Reducing Effects of Superhydrophobic Coatings. *Small* **2015** *11*, 1665-1671.
29 Cheng, M. J.; Zhang, S. S.; Dong, H. Y.; Han, S. H.; Wei, H.; Shi, F. Improving the Durability of a Drag-Reducing Nanocoating by Enhancing its Mechanical Stability. *ACS Appl. Mater. Interfaces* **2015**, *7*, 4275-4282.
30 Dong, H. Y.; Cheng, M. J.; Zhang, Y. J.; Wei, H.; Shi, F. Extraordinary Drag-Reducing Effect of a Superhydrophobic Coating on a Macroscopic Model Ship at High Speed. *J. Mater. Chem. A* **2013**, *1*, 5886-5891.
31 Liu, K.; Yao, X.; Jiang, L. Recent Developments in Bio-Inspired Special Wettability. *Chem. Soc. Rev.* **2010**, *39*, 3240-3255.
32 Pan, S., Kota, A. K., Mabry, J. M.; Tuteja, A. Superomniphobic Surfaces for Effective Chemical Shielding. *J. Am. Chem. Soc.* **2012**, *135*, 578-581.
33 Ellis, D. A., Mabury, S. A., Martin, J. W.; Muir, D. C. Thermolysis of Fluoropolymers as a Potential Source of Halogenated Organic Acids in the Environment. *Nature* **2001**, 412, 321-324.
34 Johansson, N., Fredriksson, A.; Eriksson, P. Neonatal Exposure to Perfluorooctane Sulfonate (PFOS) and Perfluorooctanoic Acid (PFOA) Causes Neurobehavioural Defects in Adult Mice. *Neurotoxicology* **2008**, *29*, 160-169.
35 Suja, F., Pramanik, B. K.; Zain, S. M. Contamination, Bioaccumulation and Toxic Effects of Perfluorinated Chemicals (PFCs) in the Water Environment: A Review Paper. *Water Sci. Technol.* **2009**, *60*, 1533-1544.
36 Mates, J. E.; Ibrahim, R.; Vera, A.; Guggenheim, S.; Qin, J.; Calewarts, D.; Waldroup, D. E.; Megaridis, C. M. Environmentally-Safe and Transparent Superhydrophobic Coatings. *Green Chem.* **2016**, *18*, 2185-2192.
37 Janjarasskul, T.; Krochta, J. M. Edible Packaging Materials. *Annu. Rev. Food Sci. Technol.* **2010**, *1*, 415-448.
38 Li, Y.; Li, L.; Sun, J. Q. Bioinspired Self-Healing Superhydrophobic Coatings. *Angew. Chem. Int. Ed.* **2010**, *49*, 6129-6133.
39 Li, Y.; Chen, S. S.; Wu, M. C.; Sun, J. Q. All Spraying Processes for the Fabrication of Robust, Self-Healing, Superhydrophobic Coatings. *Adv. Mater.* **2014**, *26*, 3344-3348.

40 Rheinwatd, J. G.; Green, H. Seria Cultivation of Strains of Human Epidemal Keratinocytes: The Formation Keratinizin Colonies from Single Cells. *Cell* **1975**, 6, 331-343.
41 Owens, D. K.; Wendt, R. Estimation of the Surface Free Energy of Polymers. *J. Appl. Polym. Sci.* **1969**, *13*, 1741-1747.
42 Kwok, D. Y.; Neumann, A. W. Contact angle measurement and contact angle interpretation. *Adv. Colloid Interface Sci.* **1999**, *81*, 167-249.
43 Koch, K.; Ensikat, H. -J. The Hydrophobic Coatings of Plant Surfaces: Epicuticular Wax Crystals and their Morphologies, Crystallinity and Molecular Self-Assembly. *Micron* **2008**, *39*, 759-772.
44 Kanokpanont, S.; Damrongsakkul, S.; Ratanavaraporn, J.; Aramwit, P. Physico-Chemical Properties and Efficacy of Silk Fibroin Fabric Coated with Different Waxes as Wound Dressing. *Int. J. Biol. Macromol.* **2013**, *55*, 88-97.
45 Reza, M. S;, Quadir, M. A.; Haider, S. S. Comparative Evaluation of Plastic, Hydrophobic and Hydrophilic Polymers as Matrices for Controlled-Release Drug Delivery. *J. Pharm. Pharm. Sci.* **2003**, *6*, 282-291.
46 Verissimo, T. V.; Santos, N. T.; Silva, J. R.; Azevedo, R. B.; Gomes, A. J.; Lunardi, C. N. In Vitro Cytotoxicity and Phototoxicity of Surface-Modified Gold Nanoparticles Associated with Neutral Red as a Potential Drug Delivery System in Phototherapy. *Mater. Sci. Eng. C* **2016**, *65*, 199-204.
47 Khetani, S. R.; Kanchagar, C.; Ukairo, O.; Krzyzewski, S.; Moore, A.; Shi, J.; Aoyama, S.; Aleo, M.; Will, Y. The Use of Micropatterned Co-Cultures to Detect Compounds that Cause Drug Induced Liver Injury in Humans. *Toxicol. Sci.* **2013**, *132*, 107-117.
48 Michalski, M.-C.; Desobry, S.; Pons, M.-N.; Hardy, J. Adhesion of edible oils to food contact surfaces. *J. Am. Oil Chem. Soc.* **1998**, *75*, 447-454.
49 Paso, K.; Kompalla, T.; Aske, N.; Rønningsen, H. P.; Øye, G.; Sjöblom, J. Novel surfaces with applicability for preventing wax deposition: a review. *J. Dispersion Sci. Technol.*. **2009**, *30*, 757-781.
50 Ashraf, M.; Foolad, M. Pre-sowing seed treatment—A shotgun approach to improve germination, plant growth, and crop yield under saline and non-saline conditions. *Adv. Agron.* **2005**, *88*, 223-271.
51 Weisensee, P. B.; Tian, J.; Miljkovic, N.; King, W. P. Water droplet impact on elastic superhydrophobic surfaces. *Sci. Rep.* **2016**, *6*, 30328.
52 Bark, D. L.; Vahabi, H.; Bui, H.; Movafaghi, S.; Moore, B.; Kota, A.K.; Popat, K.; Dasi, L. P. Hemodynamic performance and thrombogenic properties of a superhydrophobic bileaflet mechanical heart valve. *Ann. Biomed. Eng*. **2017**, *45*, 452-463.
53 Wang, W.; Salazar, J.; Vahabi, H.; Joshi-Imre, A.; Voit, W. E.; Kota, A. K.; Metamorphic Superomniphobic Surfaces. *Adv. Mater.* **2017**, 1700295.
54 Movafaghi, S.; Wang, W.; Metzger, A.; Williams, D. D.; Williams, J. D.; Kota, A. K. Tunable superomniphobic surfaces for sorting droplets by surface tension. *Lab Chip.* **2016**, *16*, 3204-3209.
55 Meuler, A. J.; Smith, J. D.; Varanasi, K. K.; Mabry, J. M.; McKinley, G. H.; Cohen, R. E. Relationships between water wettability and ice adhesion. *ACS Appl. Mater. Interfaces*. **2010**, *2*, 3100-3110.
56 Wang, W.; Lockwood, K.; Boyd, L. M.; Davidson, M. D.; Movafaghi, S.; Vahabi, H.; Khetani, S. R.; Kota, A. K. Superhydrophobic coatings with edible materials. *ACS Appl. Mater. Interfaces*. **2016**, *8*, 18664-18668.

57 Vahabi, H.; Wang, W.; Movafaghi, S.; Kota, A. K. Free-Standing, Flexible, Superomniphobic Films. *ACS Appl. Mater. Interfaces*. **2016**, *8*, 21962-21967.
58 Shibuichi, S.; Yamamoto, T.; Onda, T.; Tsujii, K. Super water-and oil-repellent surfaces resulting from fractal structure. *J. Colloid Interface Sci.* **1998**, *208*, 287-294.
59 Richard, D.; Clanet, C.; Quéré, D. Surface phenomena: Contact time of a bouncing drop. *Nature.* **2002**, *417*, 811-811.
60 Khojasteh, D.; Kazerooni, M.; Salarian, S.; Kamali, R. Droplet impact on superhydrophobic surfaces: A review of recent developments. *Ind. Eng Chem.* **2016**, *42*, 1-14.
61 Shen, Y.; Tao, J.; Chen, S.; Pan, L.; Wang, T. Approaching the theoretical contact time of a bouncing droplet on the rational macrostructured superhydrophobic surfaces. *Appl. Phys. Lett.* **2015**, *107*, 111604.
62 Bird, J. C.; Dhiman, R.; Kwon, H.-M.; Varanasi, K. K. Reducing the contact time of a bouncing drop. *Nature*. **2013**, *503*, 385-388.
63 Liu, Y.; Andrew, M.; Li, J.; Yeomans, J. M.; Wang, Z. Symmetry breaking in drop bouncing on curved surfaces. *Nat. Commun.* **2015**, *6*, 10034.
64 Liu, Y.; Moevius, L.; Xu, X.; Qian, T.; Yeomans, J. M.; Wang, Z. Pancake bouncing on superhydrophobic surfaces. *Nat. Phys.* **2014**, *10*, 515-519.

8 APPENDIX A– GENERAL LAB SUPPLEMENTARY

8.1 CSU iShip

Procedure for using CSU shipping through iShip

1. Go to http://cr.colostate.edu/main_shiprec.aspx
2. Select “Ship a Package or Large Item” icon under Shipping
3. Select iShip (unless DHL or FedEx is necessary, then fill out forms manually)
4. Login using your CSU credentials (you will need a valid Kuali number from your PI to create your account the first time you log in).
5. Select “Ship It” from the top menu.
6. Add the recipients address (if the address does not validate, request a confirmation of the address).
7. Fill out package information and a simple description of goods.
8. Select “Get Rates” once form is complete.
9. Select type of shipping (depends on time constraints and cost).
10. Finish form and print iShip form. Attach the bottom label to the package using tape.
11. Drop package off at W. Lake St. (entrance on South side of building through mailroom to back room).
12. Send tracking information to your PI.

Note: Remove **all** labels and attachments from package. Package must be completely clean of labels and attachments for CSU shipping to send the package (excluding the CSU traveler label printed from iShip and taped to package). Shipping price is typically based on weight and size of package, select appropriate package for items being shipped.

International Shipments: Look at international shipping information on http://cr.colostate.edu/main_shiprec.aspx for details and international invoice forms.

Note: Print and fill out 3 international invoice forms for international shipments.